Southeast Pacific stratocumulus in the Community Atmosphere Model

Brian Medeiros *

David L. Williamson

Cécile Hannay

Jerry G. Olson

National Center for Atmospheric Research, Boulder CO

DRAFT: last modified March 21, 2012

* *Corresponding author address:*

Brian Medeiros,

National Center for Atmospheric Research,

P.O. Box 3000,

Boulder, CO 80307-3000.

E-mail: brianpm@ucar.edu

ABSTRACT

Forecasts of October 2006 are used to investigate southeast Pacific stratocumulus in two versions of the Community Atmosphere Model (CAM4 and CAM5). Both models quickly develop biases similar to their climatic biases, suggesting that parameterized physics are the root of the climate errors. An extensive cloud deck is produced in CAM4, but the cloud structure is unrealistic because the boundary layer is too shallow and moist. The boundary layer structure is improved in CAM5, but during the daytime the boundary layer decouples from the cloud layer, causing the cloud layer to break up and transition toward a more trade-wind cumulus structure in the afternoon. The cloud liquid water budget shows how different parameterizations contribute to maintaining these different expressions of stratocumulus. Sensitivity experiments help elucidate the origins of the errors. The importance of the diurnal cycle of these clouds for climate simulations is emphasized.

1. Introduction

On synoptic spatial scales and averaged over seasons or longer, the subtropical stratocumulus decks are characterized by optically thick clouds capping a well-mixed boundary layer. These characteristics imply a strong albedo effect, and it follows that the stratocumulus decks exert a cooling influence on the climate system (Hartmann and Short 1980). The subtropical stratocumulus are found over the cool sea-surface temperatures of eastern boundary currents, and the clouds break up and transition toward cumulus-topped boundary layers over warmer water (Albrecht et al. 1995). Therefore a possibility exists for a positive feedback between the surface temperature and cloud cover, making representing stratocumulus important for coupled modeling (Duynkerke and Teixeira 2001). An underestimate in cloud cover could allow the sea-surface to warm, further reducing cloudiness (e.g., Ma et al. 1996). Stratocumulus also undergo a pronounced diurnal cycle, and because their climatic impact is manifest mostly through the shortwave radiation budget, representing this diurnal

variation is critical for capturing cloud effects on climate (see Rozendaal et al. 1995; Turton and Nicholls 1987).

Faithfully capturing subtropical stratocumulus – and other boundary layer clouds – in climate models is notoriously difficult and has been repeatedly pointed out as the largest source of uncertainty in projections of future climate (e.g., Randall et al. 2007). The prevailing difficulty is that climate models resolve scales much larger than individual clouds, necessitating parameterization. Parameterization methods are disparate, ranging from highly empirical to sophisticated cloud physics models. Evaluating these parameterizations has been hampered by incomplete observations, inappropriate comparisons, and the numerous nonlinear interactions connecting the clouds to other aspects of the simulation.

In this work, we evaluate subtropical stratocumulus in two versions of the Community Atmosphere Model (CAM4 and CAM5). Our goal is to understand the fidelity of stratocumulus in these models compared with observations and expectations. To focus on the parameterized physics, a short-term, global forecast approach is used and we restrict our analysis to the southeast Pacific (Section 2). Both models maintain stratocumulus, but show biases compared with observations. Sections 3 and 4 describe the simulated clouds, including decomposing the sources and sinks of cloud water by the parameterized processes. Model errors are discussed in Section 5, including the role of the diurnal cycle in long-term climate biases. Both models' parameterizations contain loosely constrained adjustable constants that introduce a layer of empiricism to the model physics that may influence the resulting clouds and climate. Results of sensitivity experiments that alter two of these constants are presented in Section 5. The changes impact the cloud fraction and liquid water path, but have little consequence for the processes controlling the stratocumulus. A summary and suggestions for future study are provided in Section 6.

2. Methods & Models

Stratocumulus are among the most intensely investigated cloud types, and their characteristics and environment are well described (e.g., Stevens 2005). Some aspects of stratocumulus are less well understood, such as the impacts of aerosol and mesoscale organization (e.g., Stevens and Feingold 2009). We aim to evaluate whether CAM4 and CAM5 are able to meet conceptual expectations of stratocumulus properties. To do so, we integrate the models in a forecast mode, as described next. Then we provide an overview of the models and our strategy to focus on only points that represent stratocumulus conditions.

a. Cloud-Associated Parameterization Testbed

In the Cloud-Associated Parameterization Testbed (CAPT; aka Transpose AMIP) framework, a climate model is initialized from a realistic atmospheric state, e.g., from operational numerical weather prediction analyses, over the global domain, and integrated to produce a forecast. This short-term forecast mode is useful for evaluating parameterized physics (e.g., Phillips et al. 2004; Hannay et al. 2009). Advantages of the forecast approach include: (1) avoiding some ambiguities of single-column modeling by retaining interactions between dynamics and physics, (2) being simpler and less computationally expensive to implement than full data assimilation, and (3) allowing direct comparison with observations.

In this study, forecasts are produced for each day of October 2006, with instantaneous output saved every three hours over the southeast Pacific. This period is chosen for comparison with the PreVoca Study (Wyant et al. 2010) which included development versions of CAM. The choice of year does not strongly impact conclusions regarding the processes affecting clouds in the region (the example of 2001 is briefly discussed in Section 5). The models are initialized with ECMWF analyses of wind (u, v), surface pressure (p_{sfc}), temperature (T), and specific humidity (q) that are interpolated to the CAM grid. The analyses are combined with the model's other prognostic variables (e.g., condensate and aerosol amounts

or land surface properties) from a previous integration to start a spin-up cycle in which the model is integrated forward for 6 hours. This spin-up cycle allows model variables (e.g., cloud condensate) to adjust to the analysis atmospheric state; an updated analysis state (u, v, p_{sfc}, T, q) then replaces the model-derived values to start the next 6-hour spin-up cycle. Successive spin-up cycles allow slower parts of the climate system (e.g., the land surface) to adjust to the analysis. For the results presented here the spin-up period begins from a climate run forced by prescribed SST a week prior to the forecasts. Because our focus is on the open ocean of the southeast Pacific and SST is specified, a prolonged spin-up period is not necessary, though a longer spin-up may be required when the land surface is crucial to the forecast evolution (Boyle et al. 2005). Forecasts are five-day integrations started from the spun up states at 0 UTC. Previous efforts have concluded that the starting time does not strongly impact the results (Hannay et al. 2009).

An example of the resulting forecasts is shown by Figure 6, in which the surface pressure at the location of the WHOI IMET Buoy[1] is shown for each CAM4 forecast. Some forecast skill is suggested by the similarity at overlapped times, though the sensitivity of the solution to changing initial conditions is apparent. These time series also serve as an illustration of the relatively steady conditions in the southeast Pacific during October 2006. The dominant signal apparent in the forecasts is the semi-diurnal cycle. There is no indication of spurious noise, and the forecasts appear well initialized. For comparison, the 3-hourly surface pressure from a "climate mode" integration of CAM4 is also included in Figure 6; the free-running integration shows slightly more synoptic variability than individual forecasts, but also suggests a quiescent environment throughout the month.

Figure 2 compares estimates of the low-cloud fraction and liquid water path (LWP) in the southeast Pacific from satellites and the models. Both models underestimate low-cloud fraction compared to the Multi-angle Imaging SpectroRadiometer (MISR, e.g., Marchand et al. 2010), in both October 2006 and the long-term average. There is a strong association

[1] `http://uop.whoi.edu/projects/stratus/stratus.html`

between cloud fraction and LWP in the models, but this is less apparent in the comparison of cloud fraction from MISR and LWP from the Moderate Resolution Imaging Spectrometer (MODIS, e.g., Pincus et al. submitted). We note that these comparisons should be considered qualitatively; more careful comparisons can be made with the use of satellite emulation software (see e.g., Kay et al. 2012). Averaging the second day of the October 2006 forecasts shows both models produce spatial distributions of cloud that are similar to the long-term model climatologies. Such similarity is evidence that long-term model errors are connected to the fast processes represented by the parameterized physics.

b. CAM4

Version 4 of CAM, described by Neale et al. (2010a), is similar to Version 3 (Collins et al. 2004). There are primarily three differences between the versions. First, the default dynamical core has been changed from the Eulerian spectral transform core to the finite volume core. The vertical grid used by the parameterized physics is unchanged, however, and the change of dynamical core seems to be unimportant for the issues considered here when equivalent resolutions are applied. We use the 1.9°latitude $\times$ 2.5°longitude horizontal grid with 26 vertical levels. Second, the deep convection parameterization has been modified in two ways: CAM4 uses a dilute parcel method (Neale et al. 2008) and includes convective momentum transport (Richter and Rasch 2008). Third is the inclusion of an *ad hoc* reduction of low-cloud fraction in dry conditions (called "freeze-dry"), which primarily occurs in polar regions (Vavrus and Waliser 2008).

Neither the deep convection scheme nor the "freeze-dry" cloud reduction play a role in subtropical stratocumulus, but several aspects of the remaining parameterizations are relevant for the present discussion. The boundary layer scheme is a nonlocal K-profile scheme described by Holtslag and Boville (1993). This scheme is conceptually similar to local K-profile schemes, but is reformulated to include transport of heat, moisture, and scalars from non-local dry convection. It does not include a nonlocal term for momentum, nor a

representation of turbulence generated by cloud-top radiative cooling, which is a primary energy source for stratocumulus-topped boundary layers. Effects of condensation are also excluded from the scheme, making it effectively a dry PBL parameterization. The shallow convection in CAM4 is nominally handled by the adjustment scheme of Hack (1994), which works on triplets of model levels and introduces large sensitivity to vertical resolution in CAM3 and CAM4, as demonstrated by Williamson (2012). This scheme also comes into play in stratocumulus, as discussed below and by Hannay et al. (2009). The cloud liquid (and ice) water is predicted in CAM4, but cloud fraction is diagnosed; inconsistencies between the predicted condensate and diagnosed fraction can produce "empty clouds" with large fraction and little water. The cloud fraction is diagnosed primarily through a function of relative humidity, but also through shallow and deep convection, an empirical relationship between stratus fraction and lower-tropospheric stability, and the aforementioned "freeze-dry" reduction of low-cloud. Most phase changes of water are controlled by the stratiform cloud physics described by Rasch and Kristjánsson (1998) and Zhang et al. (2003), which represent numerous macrophysical and microphysical cloud processes.

The formulation of CAM4 makes it difficult for stratocumulus to be realistically represented, as described below in detail. Indeed, these difficulties are among the motivations for changes between CAM4 and CAM5, but understanding the representation of stratocumulus in CAM4 is necessary because of its widespread use, both as an atmospheric general circulation model and also as a component in coupled climate models. This includes configurations of the Community Earth System Model (CESM) which are included in model comparison projects such as CMIP5. Versions of CAM3 and CAM4 are also the basis of the atmospheric components of other coupled modeling frameworks, such as the Beijing Climate Center model (Wu et al. 2010) and the Norwegian Earth System model (NorESM1, e.g., Zhang et al. 2012), so results from analysis of CAM4 can be extended directly to other models.

c. *CAM5*

Version 5 of CAM, described by Neale et al. (2010b), shares the finite volume dynamical core and horizontal resolution of CAM4. The vertical grid is altered: CAM5 has 30 levels rather than CAM4's 26. The additional levels are in the lower troposphere and almost double the resolution below 700 hPa. These levels improve the performance of the new boundary layer and shallow convection parameterizations in CAM5. A 30-level version of CAM4 is not supported because of biases that arise from the shallow convection formulation with increased vertical resolution in the boundary layer (Williamson 2012). The CAM5 physics parameterizations are almost entirely different from CAM4. While the deep convection scheme remains the same as for CAM4, the shallow convection and PBL schemes have been replaced with those of Bretherton and Park (2009) and Park and Bretherton (2009). In CAM5 the turbulence kinetic energy is diagnosed by the PBL scheme, which uses it to determine turbulent diffusivities. Entrainment rates are represented explicitly, and shallow convection and PBL turbulence are linked through a cloud-base mass flux. The bulk microphysics of CAM4 has been replaced with a 2-moment scheme (Morrison and Gettelman 2008), and updated cloud macrophysics – controlling conversions between condensate and water vapor at the grid-scale – improves consistency between cloud water and fraction (Park et al. in preparation). Radiative transfer is also different between the models, but the differences between the parameterizations (CAMRT and RRTMG) have a relatively small impact on tropical boundary layer clouds. Interactive aerosol is introduced in CAM5, with dust and sea-salt surface emission predicted and other emission rates prescribed; we touch on the potential role of aerosol later. The aerosol distribution is spun up in the same way as the land model. These major changes to the parameterized physics are discussed in more detail by Rasch et al. (2011) and Neale et al. (2010b).

d. Sampling stratocumulus

The structure and character of clouds in the southeast Pacific varies from thin stratus to broken cumulus, and cloud fraction typically decreases with distance from the coast (e.g., Bretherton et al. 2010). This inhomogeneity necessitates a sampling strategy to avoid conflating these different cloud types and possibly mixing different types of errors which could change the interpretation. It has been typical to define a geographical region to represent the stratocumulus deck (e.g., Klein and Hartmann 1993), but this method is inadequate for process-level studies because of the variation in cloud and boundary layer structure. Some studies of the southeast Pacific focus on a small geographic area and comparison with observations (especially at the buoy at (275°E, 20°S), e.g., Hannay et al. 2009). Others have used the transect along 20°S to show gradients in cloud structure (Wyant et al. 2010; Bretherton et al. 2010).

To understand the processes at work in the CAM4 and CAM5 forecasts, we seek a method that differentiates cloud types in the forecasts while maximizing the retained data for robust statistics. A potential complication is that we are interested in the temporal evolution of the forecasts, so we want to preserve forecasts as time series. Our approach is to classify each 5-day forecast at each grid point in the domain, and sample based on that classification. Figure 3 shows the vertical structure of grid-box mean liquid water constructed in bins of lower-tropospheric stability (LTS $\equiv \theta_{700} - \theta_{\mathrm{sfc}}$), using a $40^\circ \times 40^\circ$ domain covering the southeast Pacific (250°E–290°E, 0°–40°S). The LTS value used is the 5-day average for each forecast at each grid point for the models, and for comparison 3-day averages covering October 2006 from the ERA-Interim reanalysis. The figure suggests that mean LTS distinguishes cloud types in this region (cf. Medeiros and Stevens 2011); in both models, liquid water is found at higher levels with decreasing LTS, suggesting a weaker inversion and deeper clouds in less stable conditions. The ERA-Interim sample is qualitatively similar, though the models are biased toward less stable conditions compared to ERA-Interim; the models show larger values of liquid water amount, but note that the

liquid water path is similar between CAM4 and ERA-Interim.

To focus on stratocumulus clouds, composite forecasts are constructed by averaging the 90-95th percentiles in each model's mean LTS distribution (labeled in Figure 3). As such, the composites represent conditional averages over space and time. Although the 90th and 95th percentile values differ between the models, the sample size (6% of data) is the same. Inspecting the location and frequency of this sample (Figure 4) shows similar patterns in the models, and is consistent with ERA-Interim and expectations of the stratocumulus area (Zuidema et al. 2009); the WHOI buoy location, marked in Figure 4, is also well sampled by this strategy. Using the 95-99th percentiles (not shown) highlights a smaller area, roughly outlined in the figure by the LTS isolines $\geq$ 24 K for CAM4 and $\geq$ 22 K for CAM5. The reason for using the larger area is to avoid, as much as possible, contamination of the sample by near-coastal points that are strongly influenced by continental processes. The practical impact of this choice is minimal for our analysis. Although in CAM5 the cloud layer is slightly lower at higher mean LTS, the balance of processes forming and maintaining the cloud is similar to the discussion of Section 4. The difference in the model samples occurs because the vertical temperature structure changes over the course of the forecasts, with CAM4 tending to have warmer θ_{700} than CAM5 in the second half of the forecast. The difference is most pronounced around the periphery of the stratocumulus, where the transition to trade-wind cumulus is expected. We have explored the consequences of this sampling difference (e.g., by sampling based on mean LTS in the first 48 hours of the forecasts, in which the models' temperatures are very similar) and it has no impact on the conclusions.

3. Southeast Pacific stratocumulus in CAM4

Examining the CAM4 forecasts shows the development and maintenance of stratocumulus in the southeast Pacific. The large-scale circulation evolves slowly away from the realistic initial condition, and the circulation over the southeast Pacific is generally steady

and comparable to the analysis. Thus forecast errors are dominated by the parameterized physics. Figure 5 shows the average thermodynamic structure composited from the 90–95th percentiles of mean LTS, which we loosely define as the stratocumulus deck. Each profile shows the average over a forecast day (ending on the indicated day), so each curve represents a month-long average profile. The evolution of the profiles from day to day expresses the model adjusting away from the initial conditions. During the forecast, the PBL shallows and moistens, and is shallower and less well-mixed than *in situ* observations (Bigorre et al. 2007, dashed profiles in Figure 5). The liquid water vertical structure evolves dramatically as cloud-base descends over 2–4 days. Spatially, the model forms an extensive cloud deck (e.g., Figure 2) that slightly expands during the forecast. The temperature and humidity structures also evolve with forecast time, slowly warming and moistening the lowest model levels. The CAM4 results are similar to forecasts and climate biases in CAM3 and a preliminary version of CAM5 (Hannay et al. 2009).

Terms of the surface energy budget along with cloud and precipitation are shown in Figure 6. Dashed horizontal lines show mean values obtained during the October 2006 maintenance cruise to the WHOI buoy (precipitation statistics printed). Figure 6 suggests a stratocumulus region with extensive low-level, mostly non-precipitating clouds; the surface budget shows strong latent heat flux and downward longwave radiation. A pronounced diurnal cycle also appears, with maximum LWP near dawn and minimum in the afternoon.

The time series of Figure 6 appear to evolve through the forecast time, but much of this evolution derives from the fairly large variance associated with the changing weather conditions (even within the 90–95th percentile of LTS) and the changing locations of the sample. This variance is shown in the figure by vertical bars that denote plus/minus one standard deviation of the 3-hourly snapshots that make up the average at each forecast time. The variance in the ship-based observations can also be large, as shown by the large standard deviation of precipitation. The ship-based observations can also differ substantially from other observational estimates, for example LWP and precipitation estimates from the

Tropical Rainfall Measuring Mission (TRMM) are also shown in Figure 6. The TRMM values are discussed in more detail in Section 4, but we note here the average precipitation is 0.125 mm d^{-1}, which is more in line with the CAM4 value than the 2006 cruise average. The average LWP during the cruise (107 g m^{-2}) is also large compared to regional averages for the month from both TRMM (77 g m^{-2}) and MODIS (Figure 2, 82 g m^{-2}), while the ship-based cloud cover (70%) is somewhat less than the MISR low-cloud fraction for the month (83%). It is useful to bear in mind the spread of observational estimates as well as the variance of the sampled model data.

Even with the large variance in many of the model fields, there is a distinct and robust evolution of the cloud fraction and liquid water in the CAM4 forecasts. This evolution is seen in the vertical structure of the clouds, shown by the composite forecast in Figure 7. A layer of liquid condensate forms during the night, usually centered on the third model level ($\approx$ 929hPa). Cloud-top remains at the interface between the third and fourth ($\approx$ 867hPa) levels. Both cloud fraction and liquid water amount decrease during the daytime (sunlit hours shown by gray bars at top of the figure). The cloud fraction (contour lines in Figure 7) suggests a higher cloud-top; this illustrates the inconsistency mentioned earlier between the model's diagnostic cloud fraction parameterization and the prognostic liquid water content. Cloud-base is near the second model level ($\approx$ 970hPa) during the first hours of the forecasts; this value is lower than observations would suggest, but is not surprising given the coarse vertical resolution of CAM4. Cloud-base descends over the course of the first few days, and by about day 3 cloud-base has reached the lowest model level. This descent occurs for most forecasts, though the timing of the descent and the correspondence between cloud fraction and liquid condensate varies among forecasts. The mean behavior describes the stratocumulus deck abutting the sea surface and extending to $\approx$ 830hPa (the interface between levels), as has been shown in the model climatology (Hannay et al. 2009; Medeiros and Stevens 2011).

To better understand the adjustment from the initial state and the establishment and

maintenance of the stratocumulus, Figure 8 shows the composite forecast of the cloud liquid water budget terms, expressed as

$$\frac{\partial q_\ell}{\partial t} = \mathbf{U} \cdot \nabla q_\ell + \mathtt{T} + \mathtt{C_T} + \mathtt{C_D} + \mathtt{E} + \mathtt{P} + \mathtt{S} \tag{1}$$

Terms on the right side represent the tendencies from advection ($\mathbf{U}\cdot\nabla q_\ell$), PBL turbulence ($\mathtt{T}$), vertical transport by convection ($\mathtt{C_T}$), convective detrainment ($\mathtt{C_D}$), large-scale cloud physics (evaporation/condensation, $\mathtt{E}$), precipitation ($\mathtt{P}$), and sedimentation of cloud droplets ($\mathtt{S}$). Advection of cloud liquid is a small term, acting as a sink of liquid water from the cloud layer as the large-scale flow transports cloud water downstream toward the tropics; the magnitude is approximately proportional to the liquid water content, and it is excluded from Figure 8, leaving six tendencies that are distributed in an attempt to group sinks of cloud water from the cloud layer (top panel) and sources of cloud water to the cloud layer (bottom panel). The left side of Equation 1 is the total tendency, which is relatively small (comparable to the first contour of the individual terms) and is shown by color shading in the figure.

As in the previous figures, the diurnal cycle of cloud is prominent in Figure 8. During the nighttime, cloud forms and during the daytime it reduces. The contributing factors to this cycle are shown by the tendencies in contour lines: sources are solid contours and sinks are dashed. Adjustment away from the initial conditions appears in the liquid budget terms just as it does in the composite cloud and liquid water forecasts: this is seen in Figure 8 as a descent of the primary sources and sinks of cloud water over the first two days or so of the forecasts. The adjustment appears generally similar to the later steady state, except that there is relatively strong conversion to precipitation in the cloud layer (red contours, lower panel) contributing to the afternoon cloud dissipation the first two days.

Even CAM4's relatively simple parameterizations show the complexity of representing boundary layer clouds. The cloud deck forms through large-scale condensation during the nighttime growth of the cloud layer, complemented by detrainment of liquid water by shallow convection. Deep convection is rarely active in the stratocumulus, unlike the idealized experiment of Zhang and Bretherton (2008). Detrainment from shallow convection becomes

the largest source of liquid water to the cloud layer around midday, and remains the primary source of liquid throughout the afternoon. In the afternoon, however, large-scale evaporation within the cloud layer drives the total tendency to be negative, and the cloud layer partially dissipates as was seen in Figure 7. Partly offsetting the condensation and detrainment sources are cloud-layer sinks of liquid water by turbulent mixing (i.e., vertical diffusion), convective transport, and droplet sedimentation. In the first two days, these sinks are collocated at the heart of the cloud layer, but in the last two days sedimentation occurs in the lower half while mixing removes liquid from the upper half of the cloud layer.

At the lowest levels, the processes that remove liquid from the cloud layer become sources of liquid. The turbulent sink within the cloud layer mixes down liquid water and becomes a large source of water for the lowest levels; condensation processes are not included in the turbulent vertical diffusion, so this source is purely transport. Shallow convection often acts in concert with the turbulent mixing, transporting liquid water downward from the cloud layer and into the lowest levels. Sedimentation delivers liquid from the cloud layer to the lower layers as well. These low-level sources are mostly compensated by large-scale evaporation, but as illustrated by Figure 7, the evaporation is unable to eliminate all the liquid water, and cloud-base is maintained basically in the lowest model level. Condensation in the lowest model levels only occurs during nighttime after the PBL has become very shallow. This low cloud-base contrasts with the clear sub-cloud layer that is observed in the atmosphere below subtropical stratocumulus decks.

Figure 8 shows little activity above the fourth model level ($\approx$ 867 hPa) because there is little condensate above the cloud layer. The mean subsidence brings warm, dry air to these levels, keeping the relative humidity low (Figure 5). In the latter half of the forecasts, daytime convection impinges into this dry region, and detrained liquid water is quickly evaporated.

Even though the large-scale circulation remains fairly realistic, the forecasts show the cloud structure tending toward the preferred model state with a PBL that is too shallow.

Nevertheless, there are some realistic aspects of southeast Pacific stratocumulus in CAM4. The cloud fraction and cloud liquid maximize during nighttime and show a thinner, drier cloud layer in late afternoon, which is consistent with the observed diurnal behavior (see also Brunke et al. 2010). The terms of the surface energy budget are not out of line with observed values, and there is little precipitation from stratocumulus. The processes maintaining the stratocumulus and the diurnal variation are liquid water formation by large-scale condensation during the night, supplemented and then surpassed during the daytime by detrainment from shallow convection, which is overwhelmed in the afternoon by large-scale evaporation. The deviation from theory and observations seems to arise from the turbulence being driven only from surface fluxes, rather than by cloud-top radiative cooling; without this additional energy source, the PBL becomes too shallow and the clouds too low (see also Barrett et al. 2009).

4. Southeast Pacific stratocumulus in CAM5

The CAM5 forecasts share a number of features with the CAM4 ones, including the relatively steady circulation over the forecast periods (as in Figure 6 for CAM4) and a strong diurnal cycle. The details of the lower troposphere, however, differ in several aspects important for the stratocumulus. One of these is that the CAM5 is slightly less stable in the stratocumulus sample, so the values of mean LTS that are composited here are about 1 K lower in the CAM5 forecasts than CAM4 (discussed in Section 2.d). Based on a number of alternate sampling strategies and the agreement in location between the samples (Figure 4), this mean LTS discrepancy does not appear to cause other differences between the models. To begin to see these differences, we compare the composite stratocumulus profiles from CAM5 (Figure 9) with those discussed earlier from CAM4 (Figure 5). The thermodynamic structure in CAM5 shows a deeper and more well-mixed PBL, and the deeper PBL helps mitigate the moist bias relative to the ship-based observations (though a

small bias remains). The PBL slightly deepens during the CAM5 forecasts, differing from the collapse seen in previous model versions (e.g., Hannay et al. 2009; Wyant et al. 2010) and in CAM4 (Figure 5). Consequently, the inversion layer is better captured by CAM5. The difference in the cloud structure is striking: CAM5 maintains a clear sub-cloud layer, a cloud layer from about 930 hPa to about 860 hPa, with little overlying cloud, consistent with observations of stratocumulus (e.g., Bretherton et al. 2010). The maximum cloud water is around 0.06 g kg^{-1}, suggesting an in-cloud value of about 0.15 g kg^{-1} (because the cloud fraction is about 40% in that layer, see Figure 10). Observations suggest much larger in-cloud values, sometimes > 0.5 g kg^{-1} in stratocumulus (Wood and Field 2000); this shows that despite the improved geometry of the CAM5 cloud structure, there remain significant challenges in successfully representing boundary layer clouds. By contrast, the inconsistency between CAM4's cloud fraction and liquid condensate leads to instantaneous in-cloud liquid water content often much larger than can be supported by observations.

Figure 10 demonstrates some other differences in the CAM5 forecasts compared to CAM4 (Figure 6). The surface energy budget differs, with CAM5 having larger latent heat flux and smaller net longwave flux at the surface than CAM4. Compared to the ship-based observations, this suggests CAM5 improves the longwave flux, but might be somewhat worse in latent heat flux. The CAM5 latent heat flux is larger than that for CAM4 because the boundary layer is deeper and drier in CAM5; the near-surface relative humidity differs by about 5%, increasing evaporation from the surface. Both models have a moist bias compared to the observations, but CAM5 overestimates the latent heat flux. Examination of the contributions to the latent heat flux (LHF $= L_v \rho \|\vec{U}\| C_E (q_0 - q_*)$, where the right side is the product of the latent heat of vaporization (L_v), air density (ρ), wind speed ($\|\vec{U}\|$), the exchange coefficient (C_E), and the difference of the near-surface specific humidity (q_0) and the saturation specific humidity at the surface (q_*)) suggests that there is a difference in the exchange coefficients of the CAM formulation and that of the observations (which use the COARE algorithm, Fairall et al. 2003). The difference between the models in the net

longwave flux at the surface is primarily due to the difference in the pre-dawn minimum as CAM4 has a small diurnal cycle compared to CAM5. Since the surface temperature is similar between the stratocumulus samples in the models, the difference must be associated with downwelling longwave radiation. About 10 Wm^{-2} of difference is in the clear-sky portion of the radiation, which is likely an expression of the slightly larger column-integrated water vapor in the CAM5 forecasts. The difference in downwelling longwave radiation is largest when cloud fraction maximizes, but the difference in maximum cloud fraction between the models is small. Therefore the remaining difference in net longwave radiation is associated with differing cloud radiative properties, probably tied to the microphysics formulations and including aerosol effects in CAM5. The contribution to these differences by the different radiative transfer models – as opposed to differences in the composition of the atmosphere – is unclear.

Figures 6 and 10 also show differences in LWP, low-cloud fraction, and precipitation. While CAM4 has averages of 60 g m^{-2}, 72%, and 0.16 mm d^{-1}, CAM5 has smaller averages of 48 g m^{-2}, 63%, and 0.12 mm d^{-1}. The diurnal variation also differs: CAM4 has a peak amplitude 46% of the mean LWP and only 3% of the mean low-cloud fraction, but CAM5 has diurnal amplitudes of 57% of the mean LWP and 20% of its mean low-cloud fraction. The daily variation in precipitation differs mostly in the origin of the precipitation, with CAM4 raining more and mostly from stratiform processes while CAM5's rain is dominated by shallow convective precipitation. The ship-based observations used for Figures 6 and 10 do not adequately sample the diurnal cycle, so only the mean values are plotted (horizontal, dashed lines), and these values can differ markedly from other observational estimates as previously mentioned. To examine the diurnal cycle, we have included the composite diurnal cycle from TRMM retrievals for LWP and precipitation covering October 2006 in the region (270°E–290°E, 10°S–30°S). The approach is similar to that of Wood et al. (2002), though we construct the diurnal cycle by averaging observations for each hour and low-pass filtering to retain the diurnal and semi-diurnal harmonics of the composite series. The mean LWP is

77 g m^{-2} and the mean precipitation is 0.13 mm d^{-1}, and the normalized peak amplitude of LWP is 44% of the mean value. The mean LWP agrees well with Wood et al. (2002) (74 g m^{-2}), but the diurnal variation is much larger in the October 2006 data than the longer record of Wood et al. (2002) (they report around 30%) and the phase is earlier (peak around 03LT compared with about 06 LT). The smaller sample size of the October 2006 data probably explains most of the discrepancy, though some of the differences could be real. Based on this comparison, and keeping in mind the mean values from MODIS and the ship-based observations, it appears that both models exhibit a low bias in mean LWP, which is partly related to the overestimate of diurnal variation (especially for CAM5). Wood et al. (2002) also report that the normalized amplitude of the diurnal cycle of low cloud fraction is about half of that for LWP. This suggests CAM4 substantially underestimates cloud variation and CAM5 probably overestimates the daily variability.

The smaller cloud fraction and LWP in the CAM5 forecasts compared to CAM4 and observations are also apparent in the spatial distribution (e.g., Figure 2) and the vertical structure of the liquid water and cloud fraction (Figure 11). In comparison to CAM4 (Figure 7), the cloud layer is centered higher, cloud-base is more clearly defined, cloud-top shows more variation diurnally, and the cloud fraction and liquid water show much better correspondence with each other. The daytime breakup of the cloud deck is more pronounced, and (after day 1) the maximum cloud top reaches to nearly 850 hPa – coincident with the maximum LWP around dawn– followed by a cloud thinning during the day, with minimum cloud cover in the afternoon. Observations support some daytime cloud thinning (e.g., Wood et al. 2002), but less than CAM5 produces. The diurnal variation of cloud fraction in CAM5 with minimum cloud cover in the afternoon is suggestive of the subcloud and cloud layers becoming decoupled during the daytime, and the afternoon structure becoming more like trade-wind cumulus than homogeneous stratocumulus. The highest cloud-tops in the CAM5 forecasts occur in the early morning, however, not during the afternoon when shallow convection becomes the primary driver of cloud formation. Daytime PBL decoupling is commonly

observed in the southeast Pacific stratocumulus (cf., Jones et al. 2011), though the near disappearance of cloud appears exaggerated in CAM5.

Figure 12 shows the most important terms of the CAM5 version of Equation 1. Because of differences in the parameterizations, the definition of the terms are slightly different for CAM5: sedimentation of cloud droplets is incorporated into the microphysics term (upper panel, blue contours), and grid-scale condensation and evaporation are contained by a revised macrophysics package (lower panel, black contours). In general, cloud microphysics control conversions between cloud droplets and precipitation while cloud macrophysics control the grid-scale conversion between water vapor and cloud condensate. As in CAM4, the largest balance is between turbulent mixing (vertical diffusion) and large-scale evaporation/condensation (i.e., macrophysics). Microphysical processes are an important sink of cloud water from the cloud layer: sedimentation of cloud droplets is typically the largest component, followed by accretion and autoconversion. Mixing by convection plays a smaller role. Detrainment from shallow convection is a source of moisture to the upper half of the cloud layer and levels above the average cloud-top in the daytime. As the detrained liquid above cloud-top evaporates, levels above the stratocumulus are moistened, which can help maintain the cloud deck in the afternoon (by increasing the moisture content of entrained air). Below cloud base, the only substantial sink of liquid is through evaporation, which maximizes during the day. Thus the CAM5 stratocumulus appears to undergo a diurnal cycle in which the nighttime sees an increasing cloud fraction mostly by condensation, followed by decreasing cloud fraction during the daytime as the PBL becomes decoupled, shallow convective detrainment supplying most water to the cloud layer in the afternoon, and transitioning back to a well-mixed stratocumulus layer at nighttime as cloud-top radiative cooling once again dominates the turbulent mixing.

It is useful to note that the turbulent transport of cloud water from the cloud layer to the subcloud layer is a consequence of the model formulation. The moist turbulence (i.e., PBL) parameterization vertically transports each water constituent individually (i.e., q, q_ℓ,

q_i) based on the calculated eddy diffusivity and the vertical gradient of the transported quantity. This means these quantities are turbulently transported like conservative tracers, which explains the vertical diffusion pattern in Figure 12. This approach is consistent with other transport terms that treat the prognostic condensate like conserved quantities. The cloud macrophysics of CAM5 has been revised from CAM4 to be consistent with moisture transport (see Park et al. in preparation, for a detailed account of the revised macrophysics of CAM5). The model's parameterizations are *time split*, so each parameterization acts on the most recent modeled atmospheric state to produce a new, updated state. That updated state is passed into the next parameterization. This artificial separation of processes within the model (e.g., turbulent transport happens separately from condensation–evaporation) combined with the long model time step ($1800s$) and the associated time truncation errors means interstitial tendencies may not be analogous to observations. One example is the turbulent transport of liquid water all the way to the lowest model level, which is unrealistic. The model physics as a whole, however, conserves water and is internally consistent enough to produce a realistic atmospheric state at the end of each time step.

5. Sensitivity Experiments & Discussion

Short-term forecasts provide perspective on the southeast Pacific stratocumulus deck in CAM4 and CAM5 before long-term climate biases can form. While the large-scale circulation remains realistic throughout the forecasts, the fast processes associated with the boundary layer and clouds adjust toward a model-preferred state that is well correlated with the October climatology of both models. These fast processes slowly alter the thermodynamic state toward the model climatology as well, though the temperature and humidity, as examples, do not reach their climatological values within the 5-day forecast period. The models have been developed to capture aspects of the observed climate, yet the discrepancy in cloud structure shows that such agreement does not guarantee realistic regional features or physical phe-

nomena. This section explores the causes of the low cloud-base in CAM4 and the daytime cloud dissipation in CAM5, both of which could negatively impact climate simulations and projections. We test whether these aspects of the forecasts can be changed by choices in the parameterized physics, or whether the model formulation favors these characteristics.

Figures 5 and 7 show the rapid descent of cloud-base in CAM4 over the course of the forecasts. Since the cloud fraction and condensation both depend on relative humidity, one hypothesis for this descent is that the analysis thermodynamic structure provides a relative humidity profile that when input to the parameterized physics leads to an elevated cloud layer (as in Figure 7), but the layer descends as the model's PBL shallows and higher levels dry. We explore this hypothesis by changing the parameter in CAM4 that determines the relative humidity below which liquid water is evaporated in the lower troposphere. During the evaluation of the model physics, if predicted condensate is non-zero and the relative humidity is below this threshold, the evaporation rate is set to remove the condensate until none remains or the saturation specific humidity is reached, whichever comes first. The default relative humidity threshold is 91%, which is not sustained in the daily averages of Figure 5; Figure 13 shows results with the default value along with 80%, 85%, and 95%. We might have expected the elevated cloud layer to persist longer in the experiments with the lower threshold because of the relaxed restriction on liquid water. The experiments with the lower threshold, however, experience a similar PBL collapse and cloud-base descent as the default value (or the increased value), though the collapse is only hinted at in the model's diagnostic PBL depth and lifting condensation level (LCL, derived from the near-surface temperature and humidity) in the figure because of the coarse vertical resolution of CAM4. The reduced threshold increases cloud cover, LWP, and nighttime precipitation, and strengthens the shortwave cloud forcing. Permitting more water to condense strengthens the static stability by enhancing condensation warming in the cloud layer and evaporative cooling at lower levels (not shown). Increasing the threshold value to 95% decreases LWP and cloud fraction, but does not strongly affect PBL depth, LCL, or precipitation. These

results suggest that the shallow PBL and low cloud base in CAM4 stratocumulus results from stratifying effects of condensation in the cloud layer and evaporation in lower layers, and is robust to changes in the amount of cloud and liquid water. While these experiments are not exhaustive, we suggest that they show that the shallow PBL and low cloud-base are intrinsic in the CAM4 formulation, implying that improving lower tropospheric structure requires different boundary layer and cloud physics.

A number of studies have linked a PBL collapse such as that found in CAM4 to mechanisms for the transition from well-mixed stratocumulus to cumulus. Like the collapse in CAM4, these mechanisms often include stratifying effects of condensation and evaporation (e.g., Paluch and Lenschow 1991; Ackerman et al. 1993; Stevens et al. 1998). In CAM4, however, the PBL structure and cloud properties seem to be weakly coupled, probably because cloud processes are not directly connected with the structure of PBL turbulence.

The thinning and drying of the cloud layer during the daytime in CAM5 suggest the PBL and cloud layer frequently become decoupled. Decoupling refers to situations in which the turbulent mixing occurs in two separate layers, the cloud layer and sub-cloud layer, separated by a thin layer that is weakly stable (Nicholls 1984). In this configuration, the surface source of water to the cloud layer is removed, and the cloud layer dissipates as dry air is entrained and cloud water is evaporated. Shallow convection can connect the layers, as in the case of cumulus rising into stratocumulus, and in such cases multiple cloud-base levels can be observed (e.g., Miller et al. 1998). Figure 13 (solid, dark blue curves) hints at daytime decoupling, as the PBL top lowers in the daytime, approaching the surface LCL and cloud-base. Figure 14 also corroborates this interpretation, showing the diurnal cycle of production of turbulence kinetic energy by buoyancy (essentially the quantity $g\theta_0^{-1}\overline{w'\theta_v'}$, where g is gravitational acceleration, θ_0 is a reference temperature, and $\overline{w'\theta_v'}$ is the vertical flux of virtual potential temperature, e.g., Moeng and Sullivan 1994) averaged over the last three days of the CAM5 forecasts. The figure shows the close association of buoyancy production of turbulence kinetic energy and clouds, including during the afternoon cloud

thinning when the PBL top is close to the LCL (shown as dashed and dotted lines) in a layer of minimal buoyancy production. This layer is reminiscent of the transition layer separating the subcloud layer from decoupled stratocumulus (as discussed by Miller et al. 1998, and others). During the nighttime, the PBL depth is higher, the LCL is slightly lower, and clouds are thicker and more extensive. This diurnal cycle is consistent with observations of the diurnal cycle of stratocumulus, but the breakup in cloud cover is suggestive of cumulus below stratocumulus or even trade-wind cumulus layers.

To test whether the cloud breakup is due to the implementation of the Park and Bretherton (2009) shallow convection parameterization, we have repeated the CAM5 forecasts with a decreased efficiency for penetrative entrainment. This efficiency, like the relative humidity threshold in CAM4, has been used to adjust the global climate during CAM5 model development. Decreasing this parameter reduces the downward mixing of warm, dry free tropospheric air by shallow convection. As a result of reducing the penetrative entrainment efficiency (from 10 to 5 to 2.5), the average low-cloud fraction and LWP increase (Figure 13, light blue curves); the nighttime PBL deepens and cloud base rises, and the shortwave cloud forcing strengthens. With less vigorous mixing, the amplitude of diurnal variation increases in several quantities (e.g. LWP). There is also some indication of a change in the phase of diurnal variation, especially in low-cloud fraction, which appears to maximize slightly later in the morning. Small changes in the diurnal behavior could have a strong impact on the long-term average cloud forcing, and there are signs of this in Figure 13. Reducing the entrainment by shallow convection does not prevent the daytime thinning of the cloud layer, but may slow the cloud dissipation by increasing the nighttime liquid water content in the cloud layer. These results suggest the decoupling of the cloud and sub-cloud layers is responsible for the cloud dissipation. The transition toward a shallow-convection dominated lower troposphere in the afternoon is probably a consequence of the decoupling as the reducing cloud fraction in the morning and afternoon increases sunlight reaching the surface while the subcloud layer warms and moistens and becomes conditionally unstable to vertical

displacements. Penetrative entrainment by shallow convection is thus capable of changing cloud fraction and LWP (including their diurnal variation), but the decreased mixing does not prevent decoupling, cloud thinning, or remediate the overly large diurnal cycle.

As another test of the hypothesis that decoupling is at the root of the daytime cloud thinning in CAM5, additional forecasts were made for the 2001 EPIC period (as in Hannay et al. 2009). That period was characterized by a deep, well-mixed PBL, a strong diurnal cycle, and little cumulus convection (Bretherton et al. 2004). Applying the same analysis as presented above to the EPIC forecasts, similar conclusions are reached. The EPIC forecasts have a cooler PBL than those of 2006, and have a larger cloud fraction at all times of day. Unlike the forecasts in Hannay et al. (2009), the CAM5 PBL does not collapse, but deepens during the forecasts (as in Figure 9). The diurnal cycle is large, and there is a substantial cloud reduction during the day as in the 2006 forecasts. Comparing the PreVoca (2006) and EPIC (2001) cases shows that CAM5 frequently produces a decoupled PBL structure regardless of cloud cover, but also that the nighttime cloud cover and the magnitude of the daytime cloud dissipation may be linked to low-level temperature.

Experiments with reduced entrainment efficiency have larger cloud fraction and deeper PBL during nighttime, but the daytime cloud reduction is similar to the original CAM5 forecasts. The forecasts of the EPIC period have larger cloud fractions through the day, but the low-cloud fraction still reduces substantially during the daytime. All the simulations show evidence for a decoupled PBL mode that occurs mostly during the daytime. While the penetrative entrainment affects the mean cloud properties and diurnal cycle, these experiments show that other effects more strongly control the daytime cloud thinning. After sunrise, when the PBL becomes decoupled, the frequency of shallow convection also decreases. During these hours of reduced convection and turbulent mixing (from about 06LT to about 12LT, e.g., Figure 12), the cloud fraction decreases rapidly (Figure 11). When shallow convection begins to recover in the afternoon, detrainment of liquid into the cloud layer becomes the major source of water to the cloud layer, though cloud fraction continues

to decrease. The source of the cloud thinning is the decoupling of the cloud layer from the sub-cloud layer, removing the source of water to the cloud layer and allowing evaporation to dominate the liquid water evolution. It is difficult to diagnose decoupling from observations (cf., Jones et al. 2011), so there remains some ambiguity over whether the PBL decoupling in CAM5 is too frequent or whether the dissipation of the cloud layer is too rapid. Careful comparisons with detailed observations should be able to discriminate between the two possibilities.

6. Summary & Conclusions

Forecasts of the southeast Pacific in October 2006 have guided us toward conclusions about the parameterized physics in two versions of CAM. The short forecasts allow the dynamics to be similar to the observed atmosphere while the fast parameterized processes drive the simulation away from the realistic state. Both model versions produce a stratocumulus deck given the realistic large-scale conditions, but biases reminiscent of their climate biases emerge. In particular, CAM4 develops an extensive cloud deck with cloud-base and PBL top lower than observations show, and CAM5 produces less extensive stratocumulus but more realistic cloud-layer geometry in a deeper and more well-mixed PBL than CAM4. Both models suffer from a moist bias in the PBL, diurnal variation of LWP that is too large, and average LWP that is biased low.

The cloud liquid water budget illustrates the processes controlling the models' stratocumulus. CAM4 produces condensate by relative humidity controlled condensation and by detrainment of liquid from shallow cumulus convection. The low cloud-base is established by downward mixing of liquid water by PBL turbulence and shallow convection; condensation only occurs at the lowest model levels during nighttime after the PBL collapses. Condensation warming in the cloud layer and evaporative cooling below stratify the lower troposphere, inhibit turbulent mixing, and hasten the PBL collapse. The lack of cloud-

radiation-turbulence interactions in CAM4 are likely the ultimate cause of the PBL collapse and low cloud-base, as the model can not maintain the well-mixed PBL characteristic of subtropical stratocumulus.

Similar to CAM4, the CAM5 forecasts show the cloud water maintained by large-scale condensation and shallow convection detrainment while turbulent mixing and microphysical processes remove water from the cloud layer. A clear sub-cloud layer is maintained as liquid water mixed downward is evaporated, but the PBL remains well-mixed because cloud-top cooling provides a source of turbulence kinetic energy. During daytime, shortwave absorption in the cloud layer offsets the cloud-top cooling, allowing the cloud and sub-cloud layers to decouple and the cloud layer begins to dissipate. The magnitude of this dissipation is larger than expected compared to observations of cloud cover and LWP. The daily breakup of the stratocumulus deck could play a role in long-term biases in the subtropical stratocumulus regions in CAM5, since exaggerating the breakup reduces shortwave cloud forcing and potentially accelerates the stratocumulus-to-cumulus transition. Forecasts of October 2001 show a less frequently decoupled PBL and larger cloud fraction, but confirm that decoupled layers are associated with cloud dissipation. These results show the connection between the PBL turbulence and cloud structure, and highlight the importance of the diurnal cycle of tropical clouds in climate simulations.

Experiments that adjust constants in the parameterizations show that some characteristics of the stratocumulus region are easily altered. Allowing condensate to exist at lower relative humidity in CAM4 can increase LWP and cloud fraction and enhance shortwave cloud forcing. These changes have little impact on the vertical structure of the PBL, however. This insensitivity to cloud changes, along with inconsistencies between predicted condensate and diagnosed cloud fraction, raises concerns about the ability of CAM4 to simulate the tropical cloud response to a changing climate. In CAM5, reducing the efficiency of penetrative entrainment by shallow convection produces increased LWP and daytime cloud fraction , but the CAM5 PBL still decouples during the daytime and the diurnal cycle of cloud fraction

remains very strong. These experiments show that both model formulation and implementation are relevant for the identified errors in stratocumulus distribution and structure. We suspect the CAM4 stratocumulus is limited mainly by formulation, though, because of the insensitivity of PBL structure to parameter changes. There is some indication of an improved diurnal cycle in the CAM5 experiments, suggesting that further experimentation might lead to improved stratocumulus in climate simulations. The comparison between the 2001 and 2006 forecasts, however, might imply more frequent decoupling in warmer conditions and the potential for positive cloud feedbacks in climate simulations.

The CAM5 represents a substantial improvement in the physical representation of subtropical stratocumulus over CAM4. The possible deficiencies of stratocumulus in CAM5, i.e., the breakup of the cloud layer, should be further assessed with detailed observations and additional sensitivity experiments. One attractive avenue is to focus on the VOCALS-REx period (Bretherton et al. 2010) and compare with detailed observations of the PBL structure; preliminary analysis of forecasts for that period show similar characteristics as presented here. We have not addressed the role of aerosol in the PBL and cloud structure, but it could be substantial and comparison with observations may lead to insight about cloud-aerosol interaction. The southeast Pacific stratocumulus deck is also subject to regionally specific features, such as the daily "upsidence wave" propagating away from the continent (Garreaud and Muñoz 2004). This wave has been identified in CAM (Hannay et al. 2009), but we have not addressed it here. The role of regional features should be further considered, and the relative susceptibility of subtropical stratocumulus decks to perturbations ascertained.

Acknowledgments.

We are thankful to ECMWF for providing the analysis data. Additional ERA-Interim data were obtained through the ECMWF Data Server at `http://data-portal.ecmwf.int/`. Monthly data from MODIS and MISR were obtained electronically through the Cloud Feedback Model Intercomparison Program web site, Cloud observations for model evaluation

at http://climserv.ipsl.polytechnique.fr/cfmip-obs/. The TRMM microwave imager (TMI) data are produced by Remote Sensing Systems and sponsored by the NASA Earth Science MEaSUREs DISCOVER Project. Data are available at www.remss.com. Radiosondes and cruise data were obtained electronically from the NOAA website http://www.esrl.noaa.gov/psd/psd3/synthesis/. We also thank Sungsu Park for helpful discussion of the CAM parameterizations. This work was supported by the Office of Science (BER), U.S. Department of Energy, Cooperative Agreement DE-FC02-97ER62402. NCAR is sponsored by the National Science Foundation.

REFERENCES

Ackerman, A. S., O. B. Toon, and P. V. Hobbs, 1993: Dissipation of marine stratiform clouds and collapse of the marine boundary layer due to the depletion of cloud condensation nuclei by clouds. *Science*, **262**, 226–229.

Albrecht, B. A., C. S. Bretherton, D. Johnson, W. S. Schubert, and A. S. Frisch, 1995: The Atlantic stratocumulus transition experiment – ASTEX. *Bull. Amer. Meteor. Soc.*, **76**, 889–904.

Barrett, A. I., R. J. Hogan, and E. J. O'Connor, 2009: Evaluating forecasts of the evolution of the cloudy boundary layer using diurnal composites of radar and lidar observations. *Geophys. Res. Lett.*, **36 (17)**, doi:10.1029/2009GL038919, URL `http://dx.doi.org/10.1029/2009GL038919`.

Bigorre, S., et al., 2007: Stratus ocean reference station (20 S, 85 W): Mooring recovery and deployment cruise, R/V Ronald H. Brown Cruise 06-07, October 9–October 27, 2006. Tech. Rep. WHOI-2007-01, Woods Hole Oceanographic Institution, Woods Hole, MA 02543. URL `http://hdl.handle.net/1912/1565`.

Boyle, J. S., et al., 2005: Diagnosis of Community Atmospheric Model 2 (CAM2) in numerical weather forecast configuration at Atmospheric Radiation Measurement sites. *J. Geophys. Res.*, **110 (D15)**, doi:10.1029/2004JD005042, URL `http://dx.doi.org/10.1029/2004JD005042`.

Bretherton, C. S. and S. Park, 2009: A new moist turbulence parameterization in the Community Atmosphere Model. *J. Climate*, **22 (12)**, 3422–3448, doi:10.1175/2008JCLI2556.1, URL `http://journals.ametsoc.org/doi/abs/10.1175/2008JCLI2556.1`, `http://journals.ametsoc.org/doi/pdf/10.1175/2008JCLI2556.1`.

716 Bretherton, C. S., R. Wood, R. C. George, D. Leon, G. Allen, and X. Zheng, 2010: South-
717 east Pacific stratocumulus clouds, precipitation and boundary layer structure sampled
718 along 20 ° S during VOCALS-REx. *Atmospheric Chemistry and Physics*, **10 (21)**, 10 639–
719 10 654, doi:10.5194/acp-10-10639-2010, URL http://www.atmos-chem-phys.net/10/
720 10639/2010/.

721 Bretherton, C. S., et al., 2004: The EPIC 2001 stratocumulus study. *Bull. Amer. Meteor.*
722 *Soc.*, **85 (7)**, 967–977, doi:10.1175/BAMS-85-7-967, URL http://journals.ametsoc.
723 org/doi/abs/10.1175/BAMS-85-7-967, http://journals.ametsoc.org/doi/pdf/10.
724 1175/BAMS-85-7-967.

725 Brunke, M. A., S. P. de Szoeke, P. Zuidema, and X. Zeng, 2010: A comparison of ship
726 and satellite measurements of cloud properties with global climate model simulations
727 in the southeast Pacific stratus deck. *Atmospheric Chemistry and Physics*, **10 (14)**,
728 6527–6536, doi:10.5194/acp-10-6527-2010, URL http://www.atmos-chem-phys.net/10/
729 6527/2010/.

730 Collins, W. D., et al., 2004: Description of the NCAR Community Atmosphere Model (CAM
731 3.0). Technical note, NCAR. NCAR/TN-464+STR.

732 Duynkerke, P. G. and J. Teixeira, 2001: Comparison of the ECMWF reanalysis with FIRE I
733 observations: Diurnal variation of marine stratocumulus. *J. Climate*, **14 (7)**, 1466–1478,
734 URL http://dx.doi.org/10.1175/1520-0442(2001)014<1466:COTERW>2.0.CO;2.

735 Fairall, C. W., E. F. Bradley, J. E. Hare, A. A. Grachev, and J. B. Edson, 2003: Bulk
736 parameterization of air–sea fluxes: Updates and verification for the COARE algorithm. *J.*
737 *Climate*, **16 (4)**, 571–591, doi:10.1175/1520-0442(2003)016$⟨$0571:BPOASF$⟩$2.0.CO;2,
738 URL http://dx.doi.org/10.1175/1520-0442(2003)016<0571:BPOASF>2.0.CO;2.

739 Garreaud, R. D. and R. Muñoz, 2004: The diurnal cycle in circulation and cloudiness
740 over the subtropical southeast Pacific: A modeling study. *Journal of Climate*, **17 (8)**,

741 1699–1710, URL http://journals.ametsoc.org/doi/abs/10.1175/1520-0442(2004)
742 017<1699:TDCICA>2.0.CO;2.

743 Hack, J. J., 1994: Parametrization of moist convection in the National Center for Atmo-
744 spheric Research community climate model (CCM2). *J. Geophys. Res.*, **99**, 5551–5568,
745 doi:10.1029/93JD03478.

746 Hannay, C., D. L. Williamson, J. J. Hack, J. T. Kiehl, J. G. Olson, S. A. Klein, C. S.
747 Bretherton, and M. Köhler, 2009: Evaluation of forecasted southeast Pacific stratocumulus
748 in the NCAR, GFDL, and ECMWF models. *J. Climate*, **22 (11)**, 2871–2889, URL http:
749 //dx.doi.org/10.1175/2008JCLI2479.1.

750 Hartmann, D. L. and D. A. Short, 1980: On the use of earth radiation budget statis-
751 tics for studies of clouds and climate. *Journal of the Atmospheric Sciences*, **37 (6)**,
752 1233–1250, URL http://journals.ametsoc.org/doi/abs/10.1175/1520-0469(1980)
753 037<1233:OTUOER>2.0.CO;2.

754 Holtslag, A. A. M. and B. A. Boville, 1993: Local versus nonlocal boundary-layer
755 diffusion in a global climate model. *Journal of Climate*, **6 (10)**, 1825–1842, doi:
756 10.1175/1520-0442(1993)006⟨1825:LVNBLD⟩2.0.CO;2, URL http://journals.ametsoc.
757 org/doi/abs/10.1175/1520-0442(1993)006<1825:LVNBLD>2.0.CO;2.

758 Jones, C. R., C. S. Bretherton, and D. Leon, 2011: Coupled vs. decoupled boundary layers
759 in VOCALS-REx. *Atmospheric Chemistry and Physics Discussions*, **11 (3)**, 8431–8460,
760 doi:10.5194/acpd-11-8431-2011, URL http://www.atmos-chem-phys-discuss.net/11/
761 8431/2011/.

762 Kay, J. E., et al., 2012: Exposing global cloud biases in the Community Atmosphere Model
763 (CAM) using satellite observations and their corresponding instrument simulators. *Journal*
764 *of Climate*, doi:10.1175/JCLI-D-11-00469.1, URL http://journals.ametsoc.org/doi/
765 abs/10.1175/JCLI-D-11-00469.1.

Klein, S. A. and D. L. Hartmann, 1993: The seasonal cycle of low stratiform clouds. *J. Climate*, **6**, 1587–1606.

Ma, C.-C., C. R. Mechoso, A. W. Robertson, and A. Arakawa, 1996: Peruvian stratus clouds and the tropical Pacific circulation: A coupled ocean-atmosphere GCM study. *J. Climate*, **9 (7)**, 1635–1645, doi:10.1175/1520-0442(1996)009⟨1635:PSCATT⟩2.0.CO;2, URL http://dx.doi.org/10.1175/1520-0442(1996)009<1635:PSCATT>2.0.CO;2.

Marchand, R., T. Ackerman, M. Smyth, and W. B. Rossow, 2010: A review of cloud top height and optical depth histograms from MISR, ISCCP, and MODIS. *J. Geophys. Res.*, **115 (D16)**, doi:10.1029/2009JD013422, URL http://dx.doi.org/10.1029/2009JD013422.

Medeiros, B. and B. Stevens, 2011: Revealing differences in GCM representations of low clouds. *Climate Dynamics*, **36 (1)**, 385–399, doi:10.1007/s00382-009-0694-5, URL http://dx.doi.org/10.1007/s00382-009-0694-5.

Miller, M. A., M. P. Jensen, and E. E. Clothiaux, 1998: Diurnal cloud and thermodynamic variations in the stratocumulus transition regime: A case study using in situ and remote sensors. *J. Atmos. Sci.*, **55 (13)**, 2294–2310, doi:10.1175/1520-0469(1998)055⟨2294:DCATVI⟩2.0.CO;2, URL http://dx.doi.org/10.1175/1520-0469(1998)055<2294:DCATVI>2.0.CO;2.

Moeng, C.-H. and P. P. Sullivan, 1994: A comparison of shear and buoyancy-driven planetary boundary layers. *J. Atmos. Sci.*, **51**, 999–1022.

Morrison, H. and A. Gettelman, 2008: A new two-moment bulk stratiform cloud microphysics scheme in the Community Atmosphere Model, Version 3 (CAM3). Part I: Description and numerical tests. *J. Climate*, **21 (15)**, 3642–3659, URL http://dx.doi.org/10.1175/2008JCLI2105.1.

Neale, R. B., J. H. Richter, and M. Jochum, 2008: The impact of convection on ENSO: From a delayed oscillator to a series of events. *Journal of Climate*, **21 (22)**, 5904–5924, URL http://journals.ametsoc.org/doi/abs/10.1175/2008JCLI2244.1.

Neale, R. B., et al., 2010a: Description of the NCAR community atmosphere model (CAM 4.0). Tech. Rep. TN-485+STR, National Center for Atmospheric Research, Boulder CO, USA, 80307-3000. URL http://www.cesm.ucar.edu/models/ccsm4.0/cam/docs/description/cam4_desc.pdf.

Neale, R. B., et al., 2010b: Description of the NCAR community atmosphere model (CAM 5.0). Tech. Rep. TN-486+STR, National Center for Atmospheric Research, Boulder CO, USA, 80307-3000. URL http://www.cesm.ucar.edu/models/cesm1.0/cam/docs/description/cam5_desc.pdf.

Nicholls, S., 1984: The dynamics of stratocumulus: Aircraft observations and comparisons with a mixed layer model. *Quarterly Journal of the Royal Meteorological Society*, **110 (466)**, 783–820, doi:10.1002/qj.49711046603, URL http://dx.doi.org/10.1002/qj.49711046603.

Paluch, I. R. and D. H. Lenschow, 1991: Stratiform cloud formation in the marine boundary layer. *J. Atmos. Sci.*, **48 (19)**, 2141–2158, doi:10.1175/1520-0469(1991)048⟨2141:SCFITM⟩2.0.CO;2, URL http://dx.doi.org/10.1175/1520-0469(1991)048<2141:SCFITM>2.0.CO;2.

Park, S. and C. S. Bretherton, 2009: The University of Washington shallow convection and moist turbulence schemes and their impact on climate simulations with the Community Atmosphere Model. *J. Climate*, **22 (12)**, 3449–3469, doi:10.1175/2008JCLI2557.1, URL http://journals.ametsoc.org/doi/abs/10.1175/2008JCLI2557.1, http://journals.ametsoc.org/doi/pdf/10.1175/2008JCLI2557.1.

814 Park, S., C. S. Bretherton, and P. J. Rasch, in preparation: Global cloud simulations in the
815 Community Atmosphere Model. *J. Climate*.

816 Phillips, T. J., et al., 2004: Evaluating parameterizations in general circulation mod-
817 els: Climate simulation meets weather prediction. *Bull. Amer. Meteor. Soc.*, **85 (12)**,
818 1903–1915, doi:10.1175/BAMS-85-12-1903, URL `http://journals.ametsoc.org/doi/`
819 `abs/10.1175/BAMS-85-12-1903`, `http://journals.ametsoc.org/doi/pdf/10.1175/`
820 `BAMS-85-12-1903`.

821 Pincus, R., S. Platnick, S. A. Ackerman, R. S. Hemler, and R. J. P. Hofmann, submitted:
822 Reconciling simulated and observed views of clouds: MODIS, ISCCP, and the limits of
823 instrument simulators. *J. Climate*.

824 Randall, D., et al., 2007: Climate models and their evaluation. *Climate Change 2007: The*
825 *Physical Science Basis. Contribution of Working Group I to the Fourth Assessment Report*
826 *of the Intergovernmental Panel on Climate Change*, S. Solomon, D. Qin, M. Manning,
827 Z. Chen, M. Marquis, K. Averyt, M.Tignor, and H. Miller, Eds., Cambridge University
828 Press, Cambridge, United Kingdom and New York, NY, USA.

829 Rasch, P. J. and J. E. Kristjánsson, 1998: A comparison of the CCM3 model cli-
830 mate using diagnosed and predicted condensate parameterizations. *J. Climate*, **11 (7)**,
831 1587–1614, URL `http://journals.ametsoc.org/doi/abs/10.1175/1520-0442(1998)`
832 `011<1587:ACOTCM>2.0.CO;2`.

833 Rasch, P. J. et al., 2011: A description of the mean atmospheric climate of the Community
834 Atmosphere Model version 5 (CAM5). *J. Climate*, **in preparation**.

835 Richter, J. H. and P. J. Rasch, 2008: Effects of convective momentum transport on the
836 atmospheric circulation in the Community Atmosphere Model, Version 3. *Journal of Cli-*
837 *mate*, **21 (7)**, 1487–1499, doi:10.1175/2007JCLI1789.1, URL `http://journals.ametsoc.`

838 org/doi/abs/10.1175/2007JCLI1789.1, http://journals.ametsoc.org/doi/pdf/10.
839 1175/2007JCLI1789.1.

840 Rozendaal, M. A., C. B. Leovy, and S. A. Klein, 1995: An observational study
841 of diurnal variations of marine stratiform cloud. *Journal of Climate*, **8 (7)**,
842 1795–1809, URL http://journals.ametsoc.org/doi/abs/10.1175/1520-0442(1995)
843 008<1795:AOSODV>2.0.CO;2.

844 Stevens, B., 2005: Atmospheric moist convection. *Annual Review of Earth and Planetary Sci-*
845 *ences*, **33 (1)**, 605–643, URL http://dx.doi.org/10.1146/annurev.earth.33.092203.
846 122658.

847 Stevens, B., W. R. Cotton, G. Feingold, and C.-H. Moeng, 1998: Large-eddy simulations
848 of strongly precipitating, shallow, stratocumulus-topped boundary layers. *J. Atmos. Sci.*,
849 **55**, 3616–3638.

850 Stevens, B. and G. Feingold, 2009: Untangling aerosol effects on clouds and precipitation
851 in a buffered system. *Nature*, **461 (7264)**, 607–613, URL http://dx.doi.org/10.1038/
852 nature08281.

853 Turton, J. D. and S. Nicholls, 1987: A study of the diurnal variation of stratocumulus using
854 a multiple mixed layer model. *Quart. J. Roy. Meteor. Soc.*, **113 (477)**, 969–1009, URL
855 http://dx.doi.org/10.1002/qj.49711347712.

856 Vavrus, S. and D. Waliser, 2008: An improved parameterization for simulating Arctic
857 cloud amount in the CCSM3 climate model. *Journal of Climate*, **21 (21)**, 5673–5687,
858 doi:10.1175/2008JCLI2299.1, URL http://journals.ametsoc.org/doi/abs/10.1175/
859 2008JCLI2299.1, http://journals.ametsoc.org/doi/pdf/10.1175/2008JCLI2299.1.

860 Williamson, D. L., 2012: Dependence of APE simulations on vertical resolution with the
861 Community Atmospheric Model, Version 3. *J. Meteor. Soc. Japan*, **accepted**.

Wood, R., C. S. Bretherton, and D. L. Hartmann, 2002: Diurnal cycle of liquid water path over the subtropical and tropical oceans. *Geophys. Res. Lett.*, **29 (23)**, doi:10.1029/2002GL015371, URL http://dx.doi.org/10.1029/2002GL015371.

Wood, R. and P. R. Field, 2000: Relationships between total water, condensed water, and cloud fraction in stratiform clouds examined using aircraft data. *Journal of the Atmospheric Sciences*, **57 (12)**, 1888–1905, URL http://journals.ametsoc.org/doi/abs/10.1175/1520-0469(2000)057<1888:RBTWCW>2.0.CO;2.

Wu, T., et al., 2010: The beijing climate center atmospheric general circulation model: description and its performance for the present-day climate. *Climate Dynamics*, **34**, 123–147, URL http://dx.doi.org/10.1007/s00382-008-0487-2, 10.1007/s00382-008-0487-2.

Wyant, M. C., et al., 2010: The PreVOCA experiment: modeling the lower troposphere in the Southeast Pacific. *Atmos. Chem. Phys.*, **10 (10)**, 4757–4774, doi:10.5194/acp-10-4757-2010, URL http://www.atmos-chem-phys.net/10/4757/2010/.

Zhang, M. and C. Bretherton, 2008: Mechanisms of low cloud–climate feedback in idealized single-column simulations with the Community Atmospheric Model, Version 3 (CAM3). *J. Climate*, **21 (18)**, 4859–4878, doi:10.1175/2008JCLI2237.1, URL http://dx.doi.org/10.1175/2008JCLI2237.1.

Zhang, M., W. Lin, C. S. Bretherton, J. J. Hack, and P. J. Rasch, 2003: A modified formulation of fractional stratiform condensation rate in the NCAR Community Atmospheric Model (CAM2). *J. Geophys. Res.*, **108 (D1)**, URL http://dx.doi.org/10.1029/2002JD002523.

Zhang, Z. S., et al., 2012: Pre-industrial and mid-pliocene simulations with NorESM-L. *Geoscientific Model Development Discussions*, **5 (1)**, 119–148, doi:10.5194/gmdd-5-119-2012, URL http://www.geosci-model-dev-discuss.net/5/119/2012/.

887 Zuidema, P., D. Painemal, S. de Szoeke, and C. Fairall, 2009: Stratocumulus cloud-top
888 height estimates and their climatic implications. *J. Climate*, **22 (17)**, 4652–4666, URL
889 http://dx.doi.org/10.1175/2009JCLI2708.1.

List of Figures

1 Illustration of CAPT forecasts using CAM4 surface pressure at a single grid point in the southeast Pacific. Forecasts are initialized at 0UTC each day and extend for 5 days. Successive forecasts are shown from top to bottom, offset by 2.5 hPa; the average and range of the first forecast time series is shown by tickmarks to give a sense of scale. The bottom series is surface pressure at the same point from a CAM4 climate integration forced by SST allowed to run throughout the month. Tickmarks show the mean and range of the month-long time series; the vertical scale matches that for the forecasts. 41

2 Low-cloud fraction in grayscale and LWP as contours. The top row shows estimates for October 2006 from MISR and MODIS on the left and day-2 of the forecasts for CAM4 and CAM5 on the right. The bottom row shows the same, but for the October average over multiple years. The MISR record covers 2000–2009, and the MODIS record covers 2002–2010. The model climatologies are derived from integrations forced by observed sea-surface temperature and cover 1998–2008 for CAM4 and 1998–2005 for CAM5 (see Kay et al. 2012, for additional details). 42

3 Average liquid water in bins of 5-day mean LTS for the (top) CAM4 and (middle) CAM5 forecasts and (bottom) ERA-Interim. Bins run from 12–30 K by 0.5 K. Markers and text at the top show the data distribution by percentile; labels on the horizontal axis show corresponding values of LTS. The vertical axes show the model levels and their nominal pressure value (and ERA-Interim standard pressure levels). 43

4 Frequency of points being within the 90-95th percentile of mean LTS (color) along with the ensemble mean (time and forecasts) LTS (contours) for (left) CAM4, (middle) CAM5, and (right) ERA-Interim. The position of the WHOI IMET buoy is marked in each panel, and the 22 K contour is marked as bold. 44

5 Lower-tropospheric structure in CAM4 forecasts for the 90-95th percentiles of mean LTS. Colored profiles show averages over each forecast day for (left to right) specific humidity (g kg^{-1}), potential temperature (K), relative humidity (%), and grid-cell averaged liquid water (g kg^{-1}). Solid black curves in the left two panels show the average initial profiles interpolated from ECMWF analyses, and the dashed black curves show average profiles from rawinsondes launched during an October 2006 cruise in the same region. The vertical axis shows the model levels and their nominal pressure (hPa). 45

6 Composite forecast of surface budget terms and some cloud-relevant variables for CAM4. Top panels shows latent heat flux (light blue), sensible heat flux (dark blue), and net longwave flux at the surface (red) on the left axis, along with downward shortwave flux at the surface (orange) on the right axis. The middle panel shows low-cloud fraction (black) and liquid water path (blue), and the bottom panel shows total (dark blue shaded with vertical bars) and large-scale (light blue shaded) precipitation. Vertical bars show $\pm 1\sigma$ at each forecast time. Dashed horizontal lines show means of the ship-based observations from October 2006 (not filtered by LTS or geography). The ship-based precipitation mean and median are printed on the lower panel. Light blue, dashed, periodic curves show the diurnal cycle of TRMM estimates of LWP and precipitation. The difference between total and large-scale precipitation is the convective precipitation. 46

7 Composite forecast of cloud liquid water (color) and cloud fraction (lines) for CAM4 in the 90–95th percentiles of mean LTS. Gray bars along the top indicate the daylight hours. The vertical axis shows the model levels and their nominal pressure (hPa). 47

8 Composite forecast of CAM4 stratocumulus cloud liquid tendency. The underlying color shading is the total liquid water tendency, and the contour lines are the constituent tendencies, divided into two panels for clarity. Solid contours show positive values (sources of liquid water), and dashed contours show negative values (sinks of liquid water). The contour interval runs from -1.25—1.25 by 0.25 g kg^{-1} d^{-1} (printed at lower right). Time is shown by forecast day, beginning at 0 UTC (about 1900 LT); gray bars at the top of the upper panel mark the daylight hours. The vertical axes show the model levels and their nominal pressure (hPa). 48

9 As in Figure 5, but for CAM5. 49

10 As in Figure 6, but for CAM5. 50

11 As in Figure 7, but for CAM5. 51

12 As in Figure 8, but for CAM5's stratocumulus and the constituent contour interval is doubled to reduce the number of lines and improve clarity: they run from -1.25—1.25 by 0.5 g kg^{-1} s^{-1}. The terms of the CAM5 liquid water budget slightly differ from CAM4, as described in the text. 52

13 Composite forecasts of (top, left to right) LWP, shortwave cloud forcing (SWCF), PBL top pressure, (bottom, left to right) total precipitation rate, low cloud fraction, and lifting condensation level for CAM4 (red, dashed) and CAM5 (blue, solid). Thicker, darker curves show the default model configuration. Thin red curves show CAM4 results with alternate values of the relative humidity threshold. Thin blue curves show the CAM5 results with a reduced penetrative entrainment efficiency. 53

14 Buoyancy production (black contours) of turbulence kinetic energy in CAM5 forecasts, averaged over the last three days of the forecasts and converted to local time. Values less than 0.0002 m^2s^{-3} are shaded. Light gray contours show cloud fraction. A dotted black line shows the average LCL and a dashed black line shows the average PBL top. 54

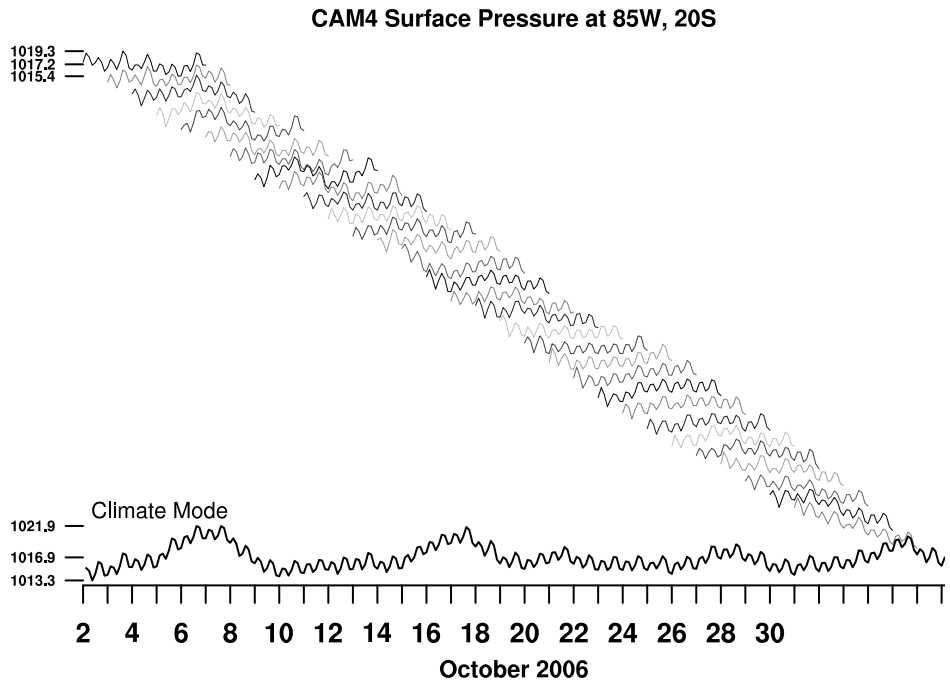

FIG. 1. Illustration of CAPT forecasts using CAM4 surface pressure at a single grid point in the southeast Pacific. Forecasts are initialized at 0UTC each day and extend for 5 days. Successive forecasts are shown from top to bottom, offset by 2.5 hPa; the average and range of the first forecast time series is shown by tickmarks to give a sense of scale. The bottom series is surface pressure at the same point from a CAM4 climate integration forced by SST allowed to run throughout the month. Tickmarks show the mean and range of the month-long time series; the vertical scale matches that for the forecasts.

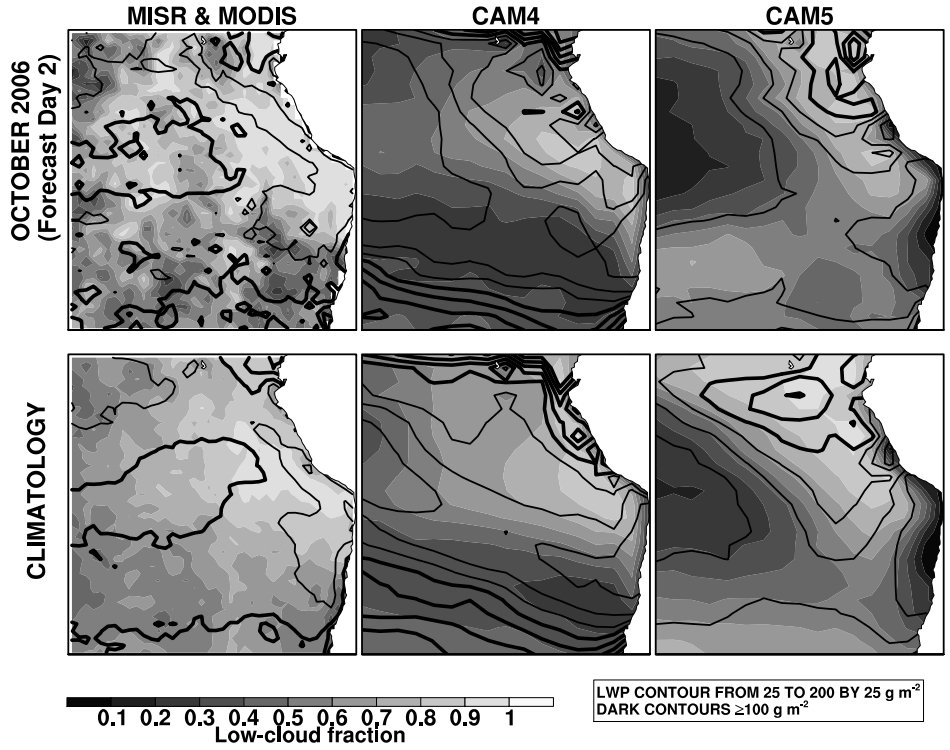

FIG. 2. Low-cloud fraction in grayscale and LWP as contours. The top row shows estimates for October 2006 from MISR and MODIS on the left and day-2 of the forecasts for CAM4 and CAM5 on the right. The bottom row shows the same, but for the October average over multiple years. The MISR record covers 2000–2009, and the MODIS record covers 2002–2010. The model climatologies are derived from integrations forced by observed sea-surface temperature and cover 1998–2008 for CAM4 and 1998–2005 for CAM5 (see Kay et al. 2012, for additional details).

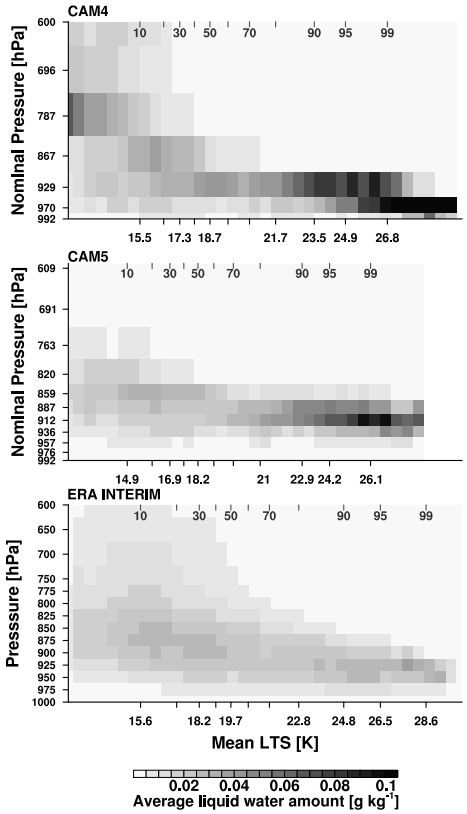

FIG. 3. Average liquid water in bins of 5-day mean LTS for the (top) CAM4 and (middle) CAM5 forecasts and (bottom) ERA-Interim. Bins run from 12–30 K by 0.5 K. Markers and text at the top show the data distribution by percentile; labels on the horizontal axis show corresponding values of LTS. The vertical axes show the model levels and their nominal pressure value (and ERA-Interim standard pressure levels).

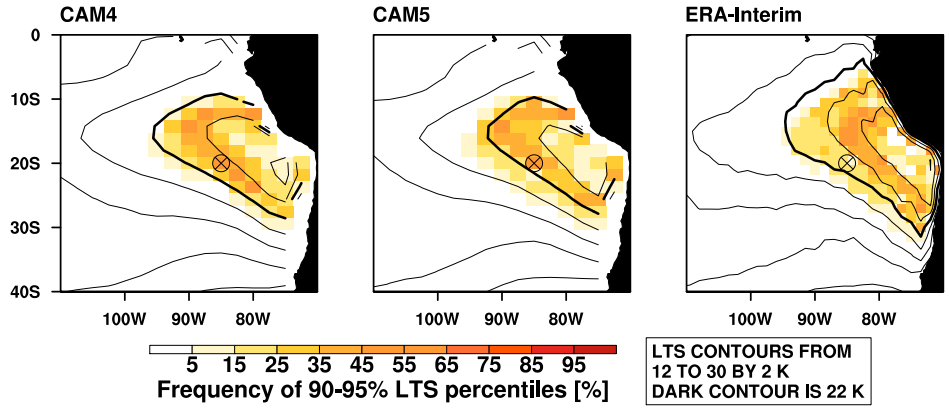

FIG. 4. Frequency of points being within the 90-95th percentile of mean LTS (color) along with the ensemble mean (time and forecasts) LTS (contours) for (left) CAM4, (middle) CAM5, and (right) ERA-Interim. The position of the WHOI IMET buoy is marked in each panel, and the 22 K contour is marked as bold.

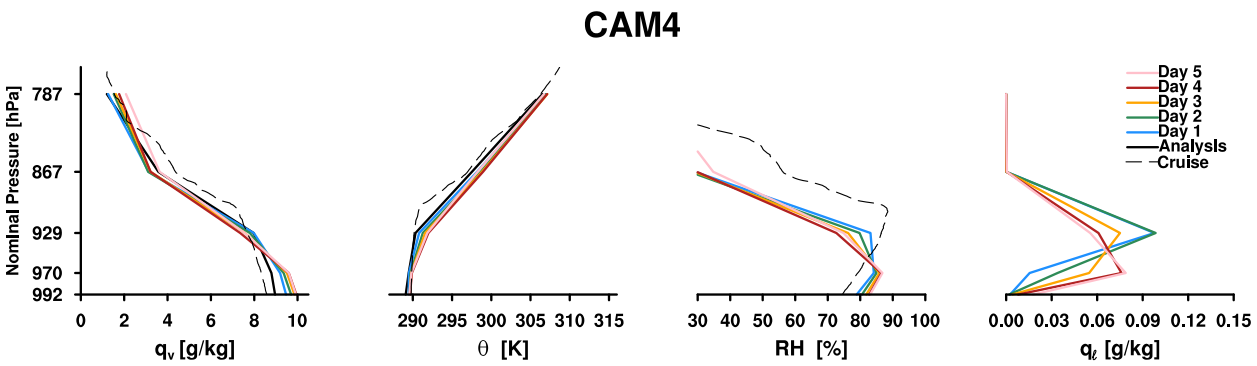

FIG. 5. Lower-tropospheric structure in CAM4 forecasts for the 90-95th percentiles of mean LTS. Colored profiles show averages over each forecast day for (left to right) specific humidity (g kg^{-1}), potential temperature (K), relative humidity (%), and grid-cell averaged liquid water (g kg^{-1}). Solid black curves in the left two panels show the average initial profiles interpolated from ECMWF analyses, and the dashed black curves show average profiles from rawinsondes launched during an October 2006 cruise in the same region. The vertical axis shows the model levels and their nominal pressure (hPa).

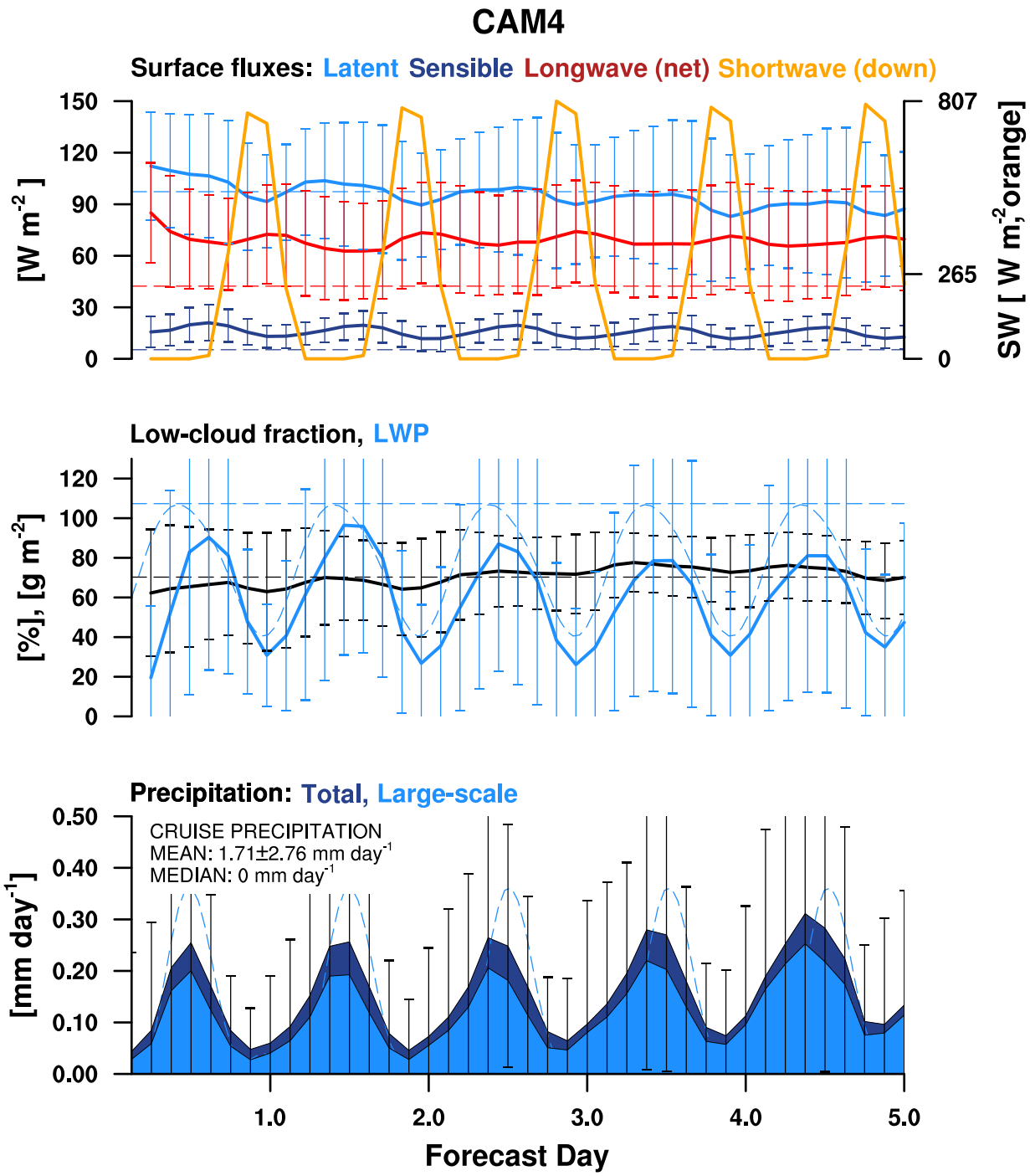

FIG. 6. Composite forecast of surface budget terms and some cloud-relevant variables for CAM4. Top panels shows latent heat flux (light blue), sensible heat flux (dark blue), and net longwave flux at the surface (red) on the left axis, along with downward shortwave flux at the surface (orange) on the right axis. The middle panel shows low-cloud fraction (black) and liquid water path (blue), and the bottom panel shows total (dark blue shaded with vertical bars) and large-scale (light blue shaded) precipitation. Vertical bars show $\pm 1\sigma$ at each forecast time. Dashed horizontal lines show means of the ship-based observations from October 2006 (not filtered by LTS or geography). The ship-based precipitation mean and median are printed on the lower panel. Light blue, dashed, periodic curves show the diurnal cycle of TRMM estimates of LWP and precipitation. The difference between total and large-scale precipitation is the convective precipitation.

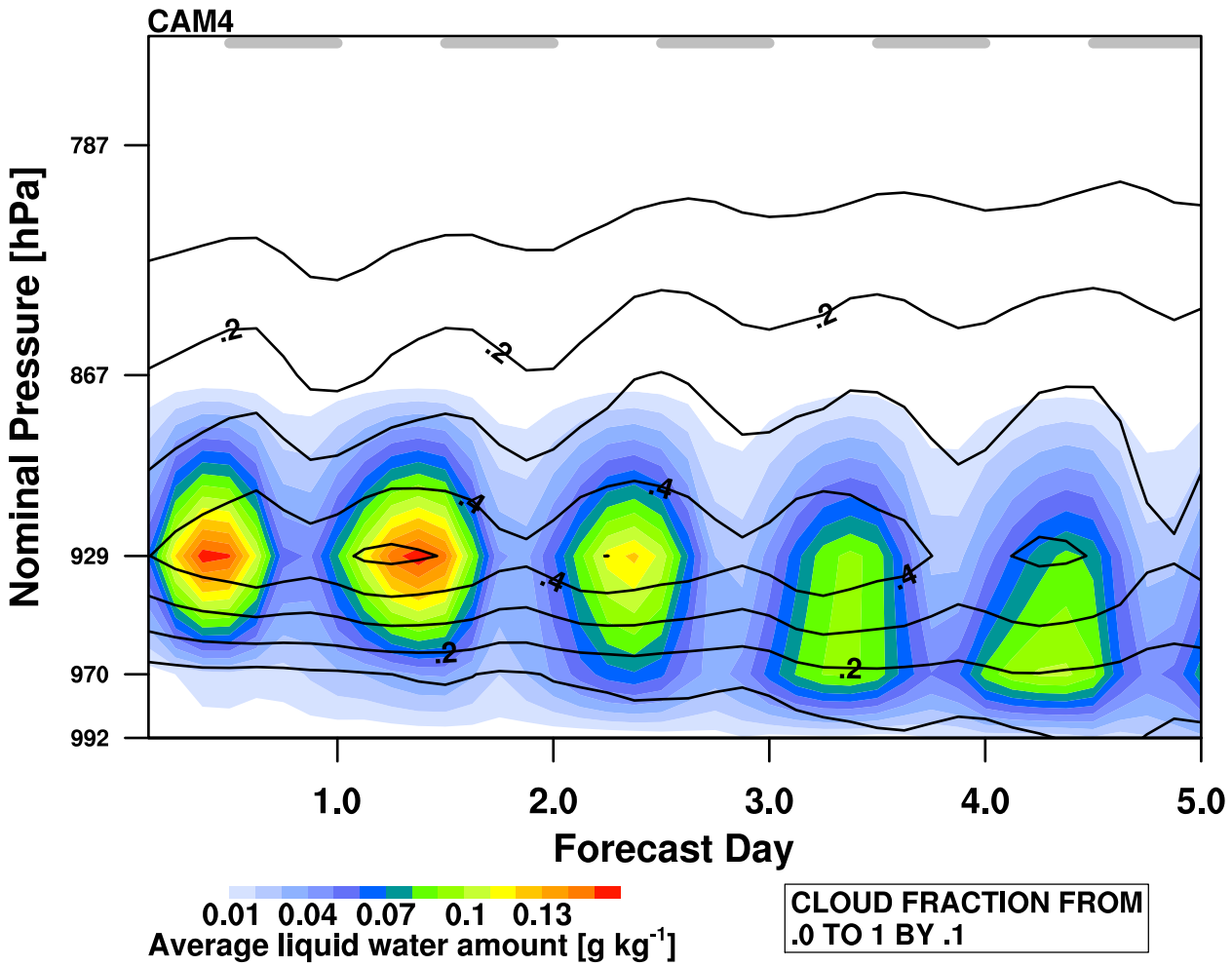

FIG. 7. Composite forecast of cloud liquid water (color) and cloud fraction (lines) for CAM4 in the 90–95th percentiles of mean LTS. Gray bars along the top indicate the daylight hours. The vertical axis shows the model levels and their nominal pressure (hPa).

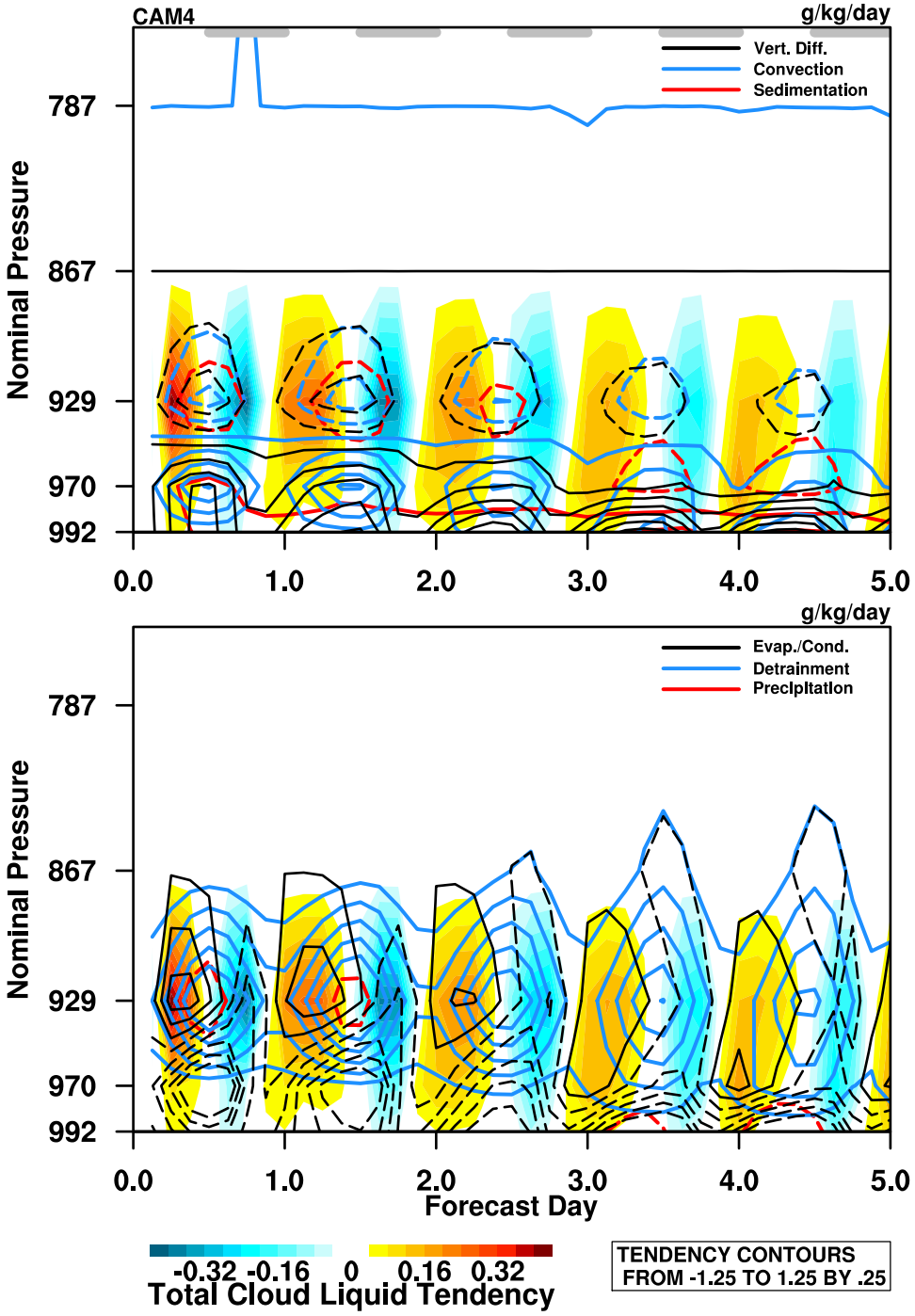

FIG. 8. Composite forecast of CAM4 stratocumulus cloud liquid tendency. The underlying color shading is the total liquid water tendency, and the contour lines are the constituent tendencies, divided into two panels for clarity. Solid contours show positive values (sources of liquid water), and dashed contours show negative values (sinks of liquid water). The contour interval runs from −1.25—1.25 by 0.25 g kg^{-1} d^{-1} (printed at lower right). Time is shown by forecast day, beginning at 0 UTC (about 1900 LT); gray bars at the top of the upper panel mark the daylight hours. The vertical axes show the model levels and their nominal pressure (hPa).

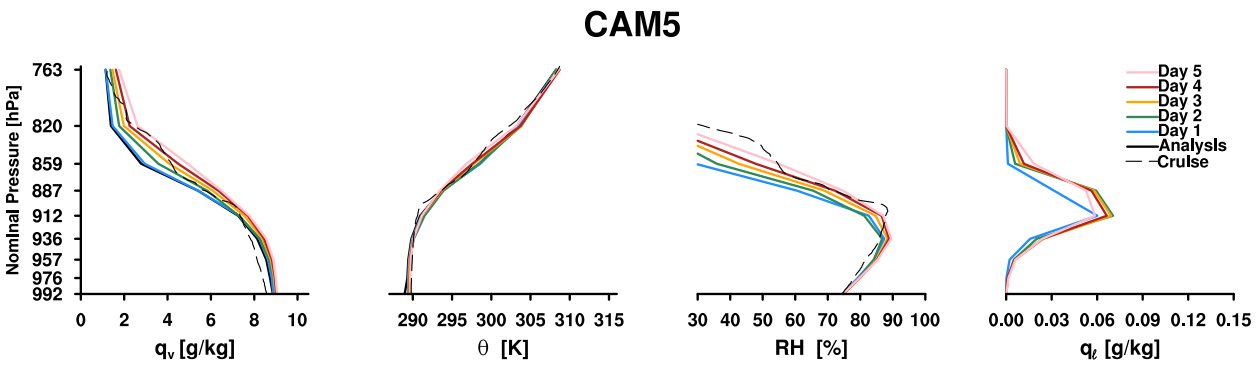

FIG. 9. As in Figure 5, but for CAM5.

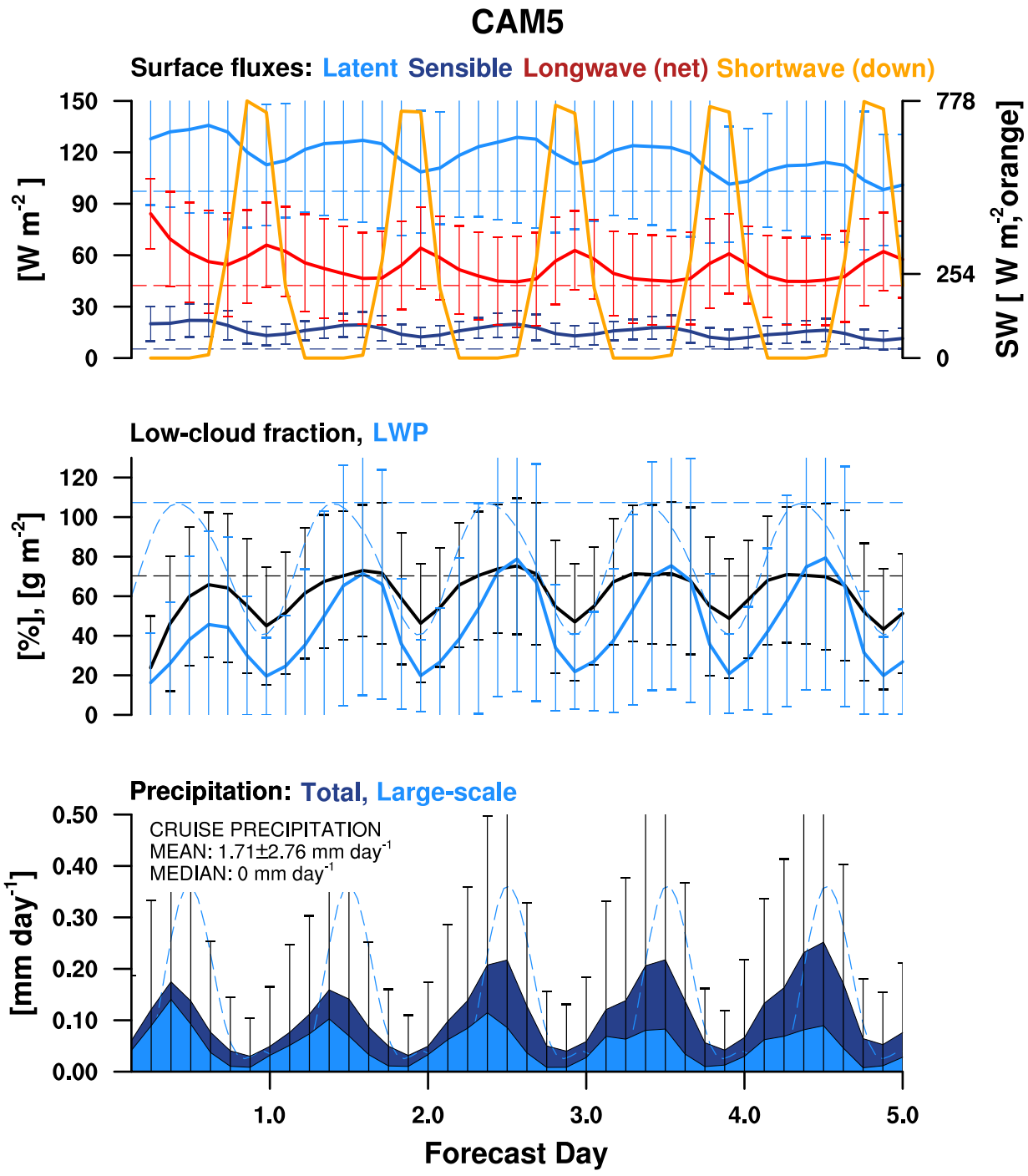

FIG. 10. As in Figure 6, but for CAM5.

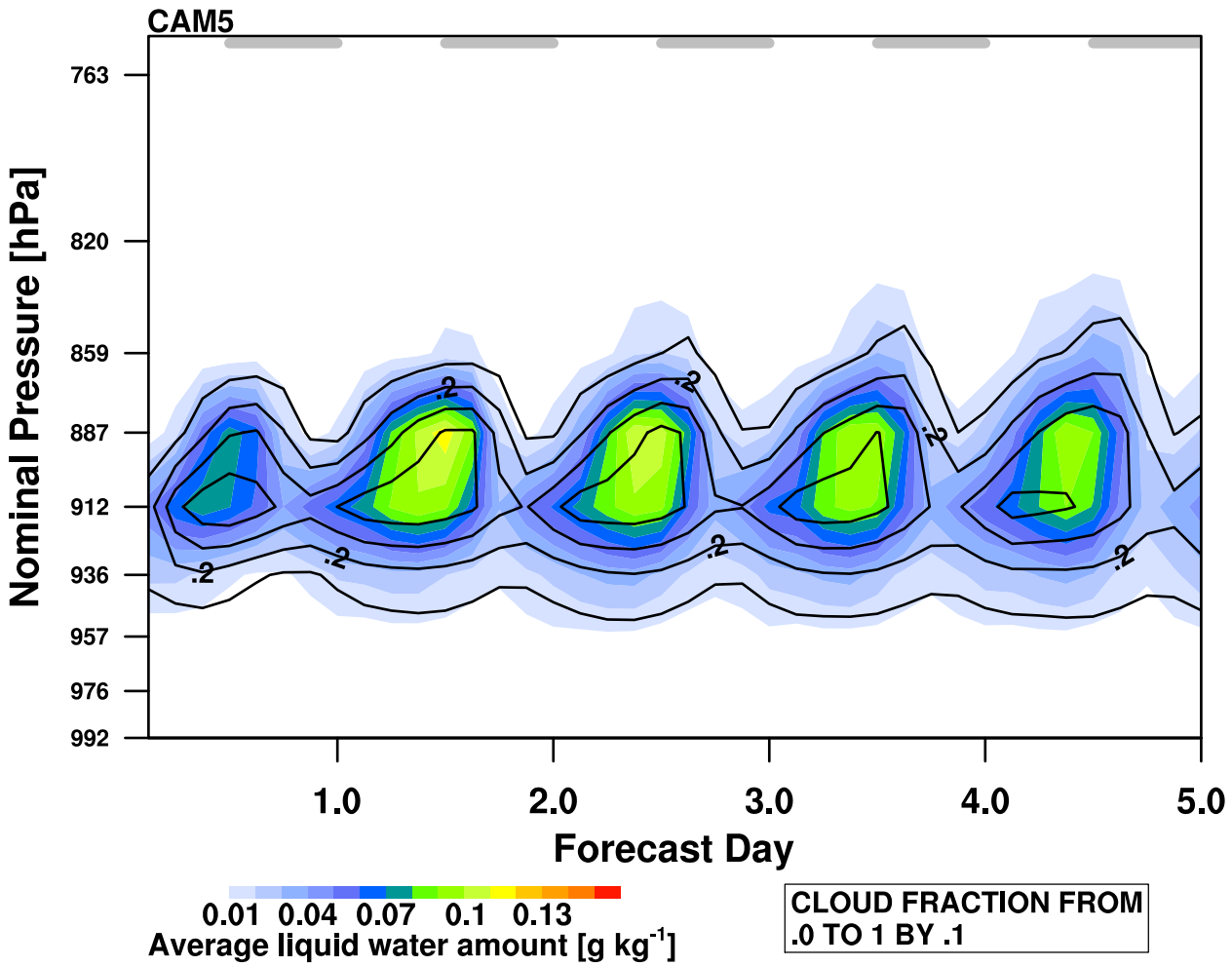

FIG. 11. As in Figure 7, but for CAM5.

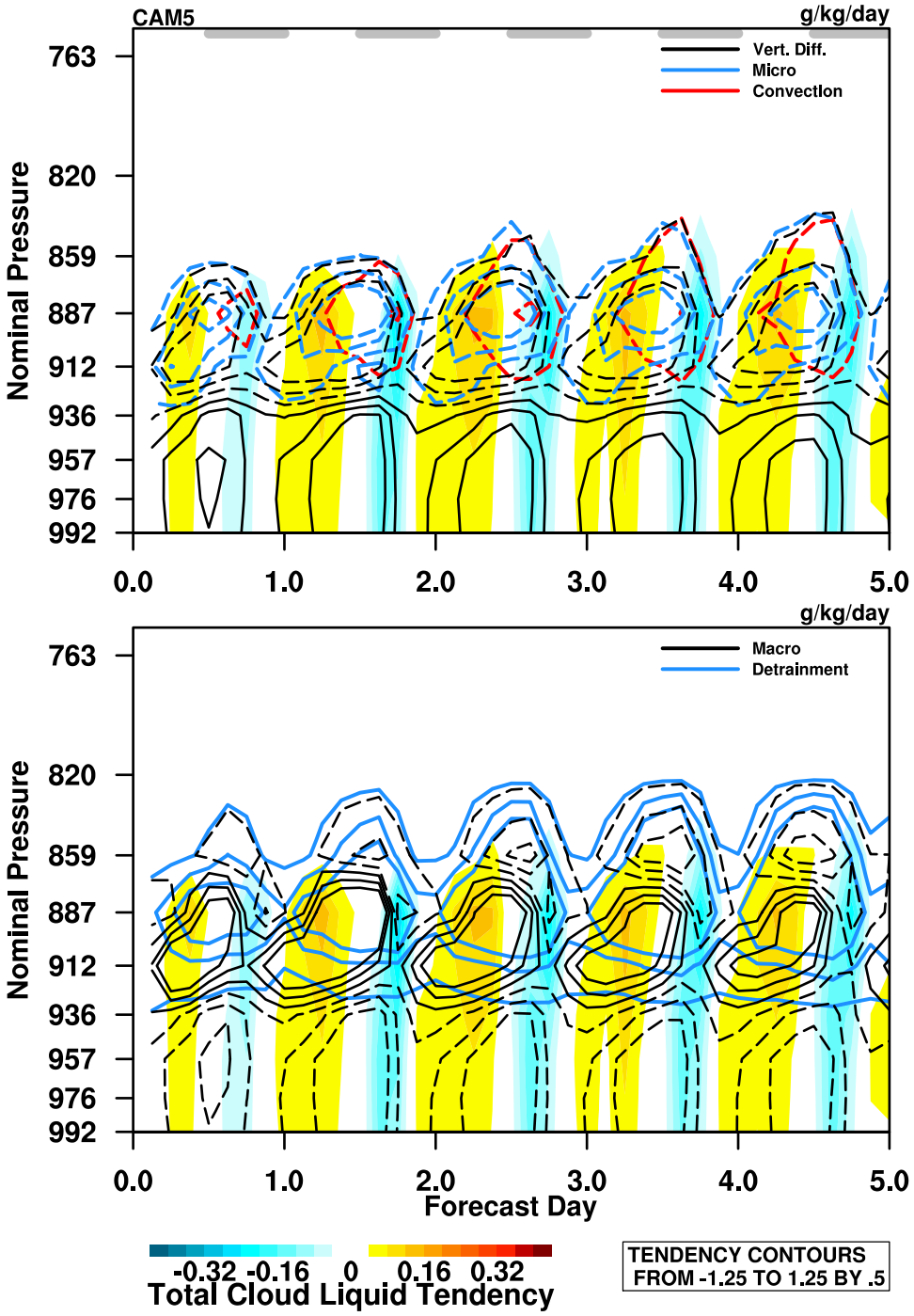

FIG. 12. As in Figure 8, but for CAM5's stratocumulus and the constituent contour interval is doubled to reduce the number of lines and improve clarity: they run from −1.25—1.25 by 0.5 g kg^{-1} s^{-1}. The terms of the CAM5 liquid water budget slightly differ from CAM4, as described in the text.

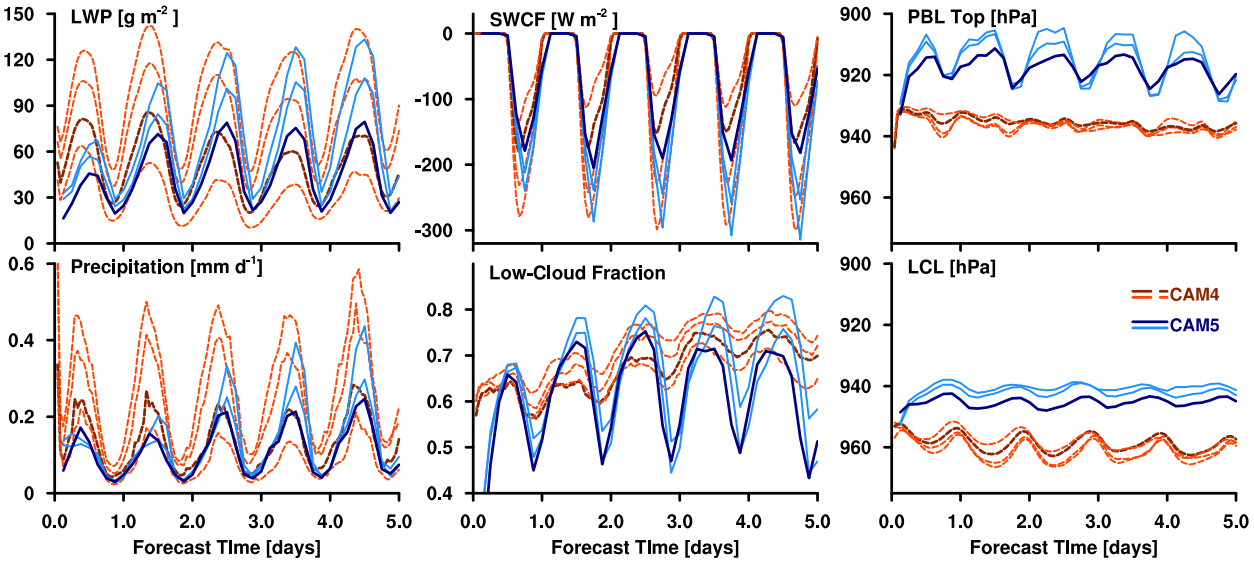

FIG. 13. Composite forecasts of (top, left to right) LWP, shortwave cloud forcing (SWCF), PBL top pressure, (bottom, left to right) total precipitation rate, low cloud fraction, and lifting condensation level for CAM4 (red, dashed) and CAM5 (blue, solid). Thicker, darker curves show the default model configuration. Thin red curves show CAM4 results with alternate values of the relative humidity threshold. Thin blue curves show the CAM5 results with a reduced penetrative entrainment efficiency.

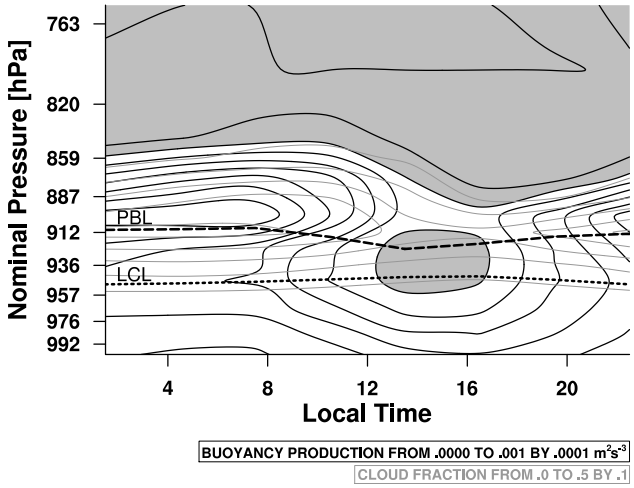

FIG. 14. Buoyancy production (black contours) of turbulence kinetic energy in CAM5 forecasts, averaged over the last three days of the forecasts and converted to local time. Values less than 0.0002 m^2s^{-3} are shaded. Light gray contours show cloud fraction. A dotted black line shows the average LCL and a dashed black line shows the average PBL top.